HHS Public Access

Author manuscript

*FASEB J.* Author manuscript; available in PMC 2021 April 01.

Published in final edited form as:

*FASEB J.* 2020 April ; 34(4): 5401–5419. doi:10.1096/fj.201902961R.

# Role of monocarboxylate transporters in regulating metabolic homeostasis in the outer retina: Insight gained from cell-specific *Bsg* deletion

**John Y. S. Han**[1], **Junzo Kinoshita**[2], **Sara Bisetto**[1], **Brent A. Bell**[3], **Romana A. Nowak**[4], **Neal S. Peachey**[2,5,6], **Nancy J. Philp**[1]

[1]Department of Pathology, Anatomy, & Cell Biology, Thomas Jefferson University, Philadelphia, PA, USA

[2]Cole Eye Institute, Cleveland Clinic, Cleveland, OH, USA

[3]Department of Ophthalmology, University of Pennsylvania, Philadelphia, PA, USA

[4]Animal Sciences, University of Illinois at Urbana-Champaign, Urbana-Champaign, IL, USA

[5]Louis Stokes Cleveland VA Medical Center, Cleveland, OH, USA

[6]Department of Ophthalmology, Cleveland Clinic Lerner College of Medicine of Case Western Reserve University, Cleveland, OH, USA

## Abstract

The neural retina metabolizes glucose through aerobic glycolysis generating large amounts of lactate. Lactate flux into and out of cells is regulated by proton-coupled monocarboxylate transporters (MCTs), which are encoded by members of the *Slc16a* family. MCT1, MCT3, and MCT4 are expressed in the retina and require association with the accessory protein basigin, encoded by *Bsg*, for maturation and trafficking to the plasma membrane. $Bsg^{-/-}$ mice have severely reduced electroretinograms (ERGs) and progressive photoreceptor degeneration, which is presumed to be driven by metabolic dysfunction resulting from loss of MCTs. To understand the basis of the $Bsg^{-/-}$ phenotype, we generated mice with conditional deletion of *Bsg* in rods (*RodΔBsg*), cones (*ConeΔBsg*), or retinal pigment epithelial cells (*RPEΔBsg*). *RodΔBsg* mice showed a progressive loss of photoreceptors, while *ConeΔBsg* mice did not display a degenerative phenotype. The *RPEΔBsg* mice developed a distinct phenotype characterized by severely reduced

**Correspondence** Nancy J. Philp, Department of Pathology, Anatomy, & Cell Biology, Thomas Jefferson University, 1020 Locust St, Philadelphia, PA 19107, USA. Nancy.Philp@jefferson.edu; Neal S. Peachey, Louis Stokes Cleveland VA Medical Center, Research Service (151), 10701 East Boulevard, Cleveland, OH 44106, USA. neal.peachey@va.gov.
**Present address** Junzo Kinoshita, Medicinal Safety Research Laboratories, Daiichi Sankyo Co., Ltd, Tokyo, Japan

AUTHOR CONTRIBUTIONS

N.J. Philp, J.Y.S Han and N.S. Peachey designed research; J. Kinoshita, M. Yu, and N.S. Peachey performed the ERGs and analyzed the data; B.A. Bell and J.Y.S. Han performed the in vivo SLO and OCT imaging and analyzed the images; J.Y.S. Han and S. Bisetto performed the histological, immunofluorescence confocal microscopy, lactate assays, PCR, and western blots and analyzed the data with N.J. Philp; R.A. Nowak generated the *Bsg*-floxed mice. J.Y.S. Han, N.J. Philp, and N.S. Peachey wrote the paper.

CONFLICT OF INTEREST

The authors declare that the research was conducted in the absence of any commercial or financial relationships that could be construed as a potential conflict of interest.

SUPPORTING INFORMATION

Additional supporting information may be found online in the Supporting Information section.

ERG responses as early as 4 weeks of age. The loss of lactate transporters from the RPE most closely resembled the phenotype of the *Bsg*$^{-/-}$ mouse, suggesting that the regulation of lactate levels in the RPE and the subretinal space is essential for the viability and function of photoreceptors.

**Keywords**

basigin; lactate; monocarboxylate transporters; photoreceptors; retina; RPE

## 1 | INTRODUCTION

The retina, composed of the neural retina and the retinal pigment epithelium (RPE), is among the most metabolically active tissues in the body and relies on glucose to support the high energy demands of visual transduction.[1,2] The RPE transports glucose from the choroid to the outer retina via GLUT1 transporters expressed in its basolateral and apical membranes.[3] In the outer retina, glucose is primarily metabolized through aerobic glycolysis, a process that produces large amounts of lactate.[3,4]

Transport of lactate within and out of the retina is mediated by monocarboxylate transporters (MCTs). MCTs differ in their affinity for lactate, which facilitates the directional flux of lactate and thus regulates metabolic coupling in the outer retina.[1] In particular, MCTs 1–4 have been characterized as proton-coupled lactate transporters[5,6] that are encoded by the *SLC16a* family, of which there are 14 known members. The neural retina expresses *Slc16a1* (encoding MCT1) and *Slc16a3* (encoding MCT4), while the RPE expresses *Slc16a1* and *Slc16a8* (encoding MCT3). The RPE expresses MCTs in a polarized manner with MCT1 expressed on the apical membrane and MCT3 expressed on the basolateral membrane. This allows for the transepithelial transport of lactate from the outer retina to the choroidal vessels.[7–12]

MCT1, 3, and 4 are nonglycosylated integral membrane protein with 12 membrane-spanning domains. These transporters form a heteromeric complex with basigin (BSG), a single pass, highly glycosylated membrane protein that is a member of the immunoglobulin superfamily and encoded by *Bsg*.[5,6] There are two isoforms of BSG, BSG1 and BSG2, which arise by an alternative splicing event.[5] Assembly of MCTs and BSG in the endoplasmic reticulum is required for proper maturation and trafficking to the plasma membrane. Previous work from our laboratory and others has shown in vitro that in the absence of one subunit, the other subunit is targeted for degradation.[10,13–15] This is similar to other heteromeric transporters, such as the $Ca^{2+}$-ATPase and amino acid transporters, where it has been shown that in the absence of the accessory protein, the transporter is targeted for degradation.[16,17]

The importance of MCTs in maintaining lactate homeostasis in the outer retina and normal visual function was demonstrated by the phenotype of the *Bsg*$^{-/-}$ mice. In this model, in the absence of BSG, MCT1, MCT3, and MCT4 were not trafficked to the plasma membrane and were instead targeted for degradation.[14] In the *Bsg*$^{-/-}$ mice, retinal development appeared normal, with proper lamination and outer segment (OS) elongation, but this normal retinal structure failed to reveal abnormalities in photoreceptor function that were apparent in the

electroretinogram (ERG).[18,19] The ERG abnormalities could be attributed to nutrient deprivation of photoreceptors from the loss of the lactate shuttle between photoreceptors and Müller cells.[14,20] Alternatively, the abnormalities could be a secondary effect due to the inability of the RPE to transport lactate and protons causing changes in pH and osmolarity in the subretinal space.[10,21,22] Lactate generated by the neural retina is a crucial substrate for oxidative phosphorylation (OXPHOS) for the RPE. When the oxidative capacity of RPE is disrupted, dedifferentiation occurs, along with subsequent photoreceptor cell death.[23–25]

Since *Bsg* is expressed throughout the retina, it has not been possible to discern whether the retinal phenotype of the $Bsg^{-/-}$ mice was from the loss of MCTs in photoreceptors, RPE, or both.[14] To understand the role of lactate transporters in supporting outer retinal function, we generated mouse lines with genetic deletion of *Bsg* from rod photoreceptors, cone photoreceptors, or the RPE. We report that the impact of *Bsg* deletion differs significantly between rods, cones, and RPE cells and that the RPE-specific deletion most closely mirrors the phenotype of the systemic $Bsg^{-/-}$, highlighting the importance of lactate transport in maintaining the homeostasis of the outer retina.

## 2 | MATERIALS AND METHODS

### 2.1 | Animal handling

Mice carrying a floxed *Bsg* allele[26] were crossed to transgenic mice expressing *Cre recombinase* in rods (B6;SJL*Pde6b*$^{+}$ Tg(Rho-iCre)1Ck/Boc JAX stock #015850)[27] or cones (Tg(Opn1mw-cre)1Asw)[28] or RPE (C57BL/6-Tg(BEST1-cre)1Jdun/J)[29] to generate mice lacking *Bsg* in rods ($Bsg^{flox/flox}$; *Rho-iCre*; hereafter *RodΔBsg*) or cones ($Bsg^{flox/flox}$; *coneCre*; hereafter *ConeΔBsg*) or RPE ($Bsg^{flox/flox}$; *Best1-Cre*; hereafter *RPEΔBsg*) and control littermates ($Bsg^{flox/+}$*Cre* positive; $Bsg^{flox/flox}$*Cre* negative; hereafter control). To generate mice lacking *Bsg* in both rod and cone photoreceptors, *ConeΔBsg* and *RodΔBsg* were crossed to generate *Cone/RodΔBsg*. To generate $MCT4^{-/-}$ mice, $MCT4^{+/-}$ mice were purchased from Taconic Bioscience. The animals were backcrossed for 10 generations to C57Bl/6J (Jackson) mice and $MCT4^{+/-}$ mice were used for breeding to obtain knock out and wild-type littermates.[30] The animals were genotyped by PCR using primers listed in Table 1. Neural retinas from 1 to 2-month-old $NRL^{-/-}$ and C57BL/6J wild-type mice were provided by the laboratories of Dr. Anand Swaroop (National Eye Institute) and Dr. Jean Bennett (University of Pennsylvania). All animal procedures were conducted with the approval of the Institutional Animal Care & Use Committees of Thomas Jefferson University, the Louis Stokes Cleveland VA Medical Center, or the Cleveland Clinic, and conformed to the ARVO statement for use of animals in ophthalmic and vision research.

### 2.2 | Western blot

Eyes were enucleated following an overdose of ketamine (100 mg/kg) and xylazine (10 mg/kg). Neural retina and RPE/choroid were isolated, and protein were extracted using 100 μL per retina and 50 μL per RPE/choroid of Pierce RIPA buffer (Cat#89900, Radioimmunoprecipitation Assay Thermo Scientific, Rockford, IL) with Halt Protease Inhibitor (Cat# 78420, Thermo Fisher Scientific, Waltham, MA). Neural retina samples were homogenized first with an 18-G Sterile needle (Cat#305195, BD PrecisionGlide Needle,

Franklin Lakes, NJ) and then a 25-G Sterile needle (Cat#305124, BD PrecisionGlide Needle). Samples were placed on ice for 30 minutes with intermittent vortexing. The protocol for enriching the RPE protein or the RPE/choroid protein isolation has previously been described.[31] In short, eyecups were isolated and four cuts were made to flatten each eyecup before it was placed in RIPA buffer and agitated to release the RPE. The supernatants were transferred to new tubes. The tubes were flicked every 10 minutes for 30 minutes after which samples were centrifuged at 14 000×*g* for 30 minutes, and the supernatants removed for protein quantification by BCA Protein Assay Kit (Cat#23225, ThermoFisher). A total of 5 or 15 μg (retina) or 5 μg (RPE/choroid) protein was loaded on 4%–12% NuPage Bis-Tris Protein gels (NP0321BOX, Invitrogen, Carlsbad, CA) or 10% NuPage Bis-Tris Protein gels (Cat# NP0301BOX, Invitrogen). Gels were run for 50 minutes at 200V per manufacturer instructions. Gels were transferred electrophoretically onto EMD Millipore Immobilon-P PVDF Transfer Membranes (Cat# IPVH00010, EMD Milipore, Burlington, MA) at 20V for 1 hour. Membranes were incubated for 1 hour at room temperature in blocking buffer (5% low fat powdered milk in Tris-buffered saline with 0.1% Tween20 [TBST]) and incubated overnight with antibodies at 4°C in blocking buffer TBST. Membranes were washed three times with DI water and incubated for 1 hour with secondary antibody in blocking buffer at room temperature. Blots were developed using chemiluminescence (Cat# 34075, SuperSignal West Dura, Thermo Fisher Scientific) on FluorChem M Protein Simple (San Jose, CA) detection system.

### 2.3 | PNGaseF treatment

Retina lysates from control and *NRL*$^{-/-}$ mice were prepared as described above. Lysates were treated with PNGaseF following the manufacture's protocol (Cat# P0704S, New England BioLabs, Ipswich, MA). Briefly, 10 μg of protein and 1 μL of glycoprotein denaturing buffer were combined in a 1.5-mL tube and brought up to 10 μL of volume with deionized water ($dH_2O$). Proteins were denatured at 100°C for 10 minutes and centrifuged for 10 seconds at 10 000×*g* at 4°C. After addition of 2 μL of GlycoBuffer 2, 2 μL of 10% NP-40, 1 μL of PNGaseF, and 6 μL of $dH_2O$ tubes were incubated in a 37°C water bath for 1 hour. SDS sample buffer was added to the tubes, and proteins were resolved by SDS-PAGE and western blot as described above. Blots were probed with BSG antibody.

### 2.4 | Co-immunoprecipitation

The procedure for co-immunoprecipitation was previously described.[15] In short, retinas were lysed in ice-cold lysis buffer (50 μL/retina [25 mM HEPES buffer, pH 7.4], 150 mM NaCl, 5 mM $MgCl_2$, 1% CHAPS detergent) containing protease inhibitor Halt Protease Inhibitor (Cat# 78420, Thermo Fisher Scientific) in each tube. The lysate was spun down at 14 000×*g* at 4°C for 30 minutes. Afterward, 10 μL of each tube was set aside for lysate control for immunoblotting. The remaining lysate was divided equally into two tubes to be incubated with 1 μL of MCT1 or MCT4 overnight at 4°C. Then 25 μL of Pierce Protein A/G Magnetic Beads (Cat#88802, Thermo Fisher Scientific) was added to the samples for 1 hour. The samples were isolated by using DynaMag-2 Magnet (Cat#12321D, Thermo Fisher Scientific). The samples were washed in lysis buffer, and then resuspended in 2×LDS sample buffer and analyzed by immunoblotting.

### 2.5 | Tissue preparation and immunofluorescence

Mice were euthanized, and the eyes were enucleated and immediately placed into 4% paraformaldehyde (PFA) (Cat#15710, Electron Microscopy Sciences, Hatfield, PA) for 2 minutes. The eyes were placed in 1× PBS and the cornea was removed. Eyecups with the lens intact were placed in 1 mL of 4% PFA for 2 hours at room temperature on a rocker. The lens was then removed, and the remaining eyecup was washed in 1× PBS three times. The eyecup was put through a sucrose gradient from 5% to 30% in a stepwise manner. Samples were frozen in Neg-50 Frozen Section Medium (Cat# 6502, Thermo Fisher Scientific), and cryosections (10-μm thick) were collected and stored at –80°C.

For immunofluorescence confocal microscopy, frozen sections were brought to room temperature, and a hydrophobic barrier was drawn around the samples on the slide using an ImmEdge Hydrophobic Barrier PAP Pen (Cat# H-400, Vector Laboratories, Burlingame, CA). 1× PBS was used to wash away the Neg-50 Frozen Section Medium and sections were blocked in PBS with 5% BSA and 0.1% Tween 20 (PBST) for 1 hour at room temperature. Antibodies were diluted in PBST containing 1% BSA (see Table 2 for antibody dilutions), and sections were incubated with the primary antibodies overnight at 4°C. The slides were washed three times in PBST and then incubated with the appropriate secondary antibodies diluted in 1% BSA PBST for 30 minutes. Slides were then washed three times in PBST and once in PBS, then incubated with 4′,6-diamidino-2-phenylindole (DAPI) for 10 minutes to label nuclei. Slides were washed twice in PBS and coverslips were mounted with Gelvatol. Slides were imaged on an LSM 780 NLO laser scanning microscope (Carl Zeiss, Oberkochen, Germany) using ApoPlan ×63/1.4 objective and EC NeoPlan ×10/0.3 objective.

### 2.6 | RNA and cDNA

Neural retinas were isolated and placed immediately into 1-mL TRIzol (Cat# 15596026, Thermo Fisher Scientific) after which they were homogenized with a 1-mL syringe with an 18-G needle (Cat# 305195, BD PrecisionGlide Needle) then with a 25-G needle (Cat#305124, BD PrecisionGlide Needle). RNA was extracted according to manufacturer specifications. RNA was quantified on NanoDrop (Cat#ND-1000, Thermo Fisher Scientific). RNA (1 μg) was reverse transcribed to 20-μL cDNA using EcoDry Premix ([oligo dT] Cat# 639543 Takara Bio USA, Mountain View, CA).

### 2.7 | Quantitative PCR

cDNA of mRNA derived from 1 μg of total RNA was used for RT-PCR. mRNA (1 μg) was amplified from 1 μg of total RNA. qPCR was done using 10 ng of cDNA, and PowerUp SYBR Green Master Mix (Cat#A25742, ThermoFisher Scientific) on a QuantStudio 5 Real-Time PCR System (Cat#A28139, ThermoFisher Scientific). The PCR reaction was done according to manufacturer's protocol, using primers listed in Table 2. In brief, reactions were heated to 50°C for 2 minutes and held to 95°C for 10 minutes. Samples were then denatured at 95°C. Cycle threshold ($C_t$) values were generated by the software and normalized to RPLP0, and $2^{-(\Delta Ct)}$ values were used to compare gene expression.

### 2.8 | Flatmounts for RPE

The procedure for RPE flatmounts were performed as previously described.[3] Eyes were isolated from euthanized mice and fixed in 4% PFA for 8 minutes in a 96-well plate, after which they were transferred to a well with 1x Dulbecco's phosphate-buffered saline (DPBS) (Cat# 21–030-CM, Corning, Corning, NY). Extraocular muscles and connective tissues attached to each eye were removed using fine forceps and scissors. The anterior segment of the eye was removed using a razor blade and the retina was dissected using fine forceps. The posterior eyecup was fixed again in 4% PFA for 8 minutes and subsequently washed with 1× DPBS. The fixed eyecup was permeabilized in 0.3% Triton X-100 in 1× DPBS for 15 minutes and blocked with 5% BSA and 0.1% Triton X-100 for 1 hour. The eyecups were incubated in primary antibody overnight in a well in 1% BSA 0.1, %Tween 20, 0.1% Triton X-100 and washed in 1× DPBS (Table 2). Eyecups were then incubated at room temperature with secondary antibody in 1% BSA, 0.1% Tween20, and 0.1% Triton X-100 for 1 hour and then washed in 1× DPBS and transferred to a well with DAPI and 0.1% Triton X-100 for 1 hour. Eyecups were finally washed in 1× DPBS and were placed on glass slides. A hydrophobic pen was used to draw a circle around the eyecup, and 1× DPBS was used to slightly suspend the eyecup with the RPE side facing upward. To flatten the eyecup, 4–8 radial cuts were made, and a Kimwipe was used to gently wick away the 1× DPBS. Gelvatol was used as a mounting medium for the coverslip. Flatmounts were imaged using a Nikon (Melville, NY) Eclipse E800 fluorescent microscope using the Plan Fluor 10×/0.30 or 40×/0.75 objectives.[3]

### 2.9 | Confocal scanning laser ophthalmoscopy (cSLO) and spectral domain optical coherence tomography (SD-OCT)

Mice were anesthetized with ketamine (100 mg/kg) and xylazine (10 mg/kg) and eyes were anesthetized with 0.5% proparacaine HCl ophthalmic solution (NDC: 17478-263-12 Akorn, Lake Forest, IL). Pupils were dilated with 1% tropicamide eye drops (NDC: 17478-102-12 Akorn). Ocular eye shields[32,33] and Systane Ultra Lubricant Eye Drops (Alcon Laboratories Fort Worth, TX) were used to keep eyes hydrated. cSLO images were obtained using a Spectralis HRA+OCT (Heidelberg Engineering, Franklin, MA). Mice were positioned with the optic nerve in the center of the image using a 55° field of view (FOV) lens and imaged with two different modes, Infrared reflectance (IR) and blue autofluorescence (BAF). Following cSLO, SD-OCT imaging was conducted using a Bioptigen Envisu R2210 system (Leica Microsystems, Buffalo Grove, IL). A 50- FOV objective lens was used to image the posterior pole, which provided a 1.4-mm diameter view of the mouse retina. Orthogonal B-scans (1000 A-Scans/B-scan) of the horizontal and vertical meridians were collected with the optic disk centrally located and averaged over 15 frames. ImageJ 1.52i was used to analyze images for outer nuclear layer (ONL) thickness and inner segment and OS thickness (photoreceptor layer [PL]), and to quantify BAF images. Animals were imaged between 4 and 35 weeks of age.

All images on the cSLO were acquired with the auto-normalization activated, which provided the best contrast. The normalization feature performed a histogram stretch on every image collected normalizing to the brightest and darkest pixels in image and assigning them to the 255 and 0 gray intensity levels, respectively. As a result, images without substantial

autofluorescence appear bright since the lipofuscin autofluorescence originating from the RPE is the brightest entity within the image. The background in the control and mutant images gets enhanced or suppressed, respectively, relative to the brightness of objects within the field of view. Mice without any appreciable autofluorescence signal will appear bright due to the auto-normalization correction, but in images with numerous bright objects, the background gets pushed down and appears darker. These bright objects are referred to as hyperfluorescent foci (HF).

### 2.10 | Lactate assay

Krebs-Ringer-Bicarbonate (KRB) was made containing (98.5 mM NaCl, 4.9 mM KCl, 1.2 mM $KH_2PO_4$, 1.2 mM $MgSO_47H_2O$, 20 mM HEPES, 2.6 mM CaCl-$2H_2O$, 25.9 mM $NaHCO_3$). All components were dissolved in deionized $H_2O$ and 5% $CO_2$ was used to bring KRB to a 7.4 pH. KRB was filtered through a 0.22-μm membrane. Glucose was added to KRB solution and the final concentration was 5 mM. KRB with 5mM of glucose was aliquoted into 48-well plates (Cat# 3548, Corning, NY) and placed into a 37-C cell incubator under 5% $CO_2$ before dissection and the rest of KRB with 5 mM of glucose was placed on ice in a 35-mm dish for the retina dissections. Neural retinas were dissected from mice and immediately put in KRB with 5 mM of glucose. Single retina was placed in a well of a 48-well plate that was previously placed in the 37-C cell incubator. Lactate released was measured at 30 minutes using the Lactate Reagent (Cat# 73510, Trinity Biotech, Bray, Co Wicklow, Ireland) according to manufacturer protocol and graphed relative to control.

### 2.11 | ERG—methods and analysis

Control and mutant mice were tested at ages ranging from 4 to 35 weeks. After overnight dark adaptation, mice were anesthetized with ketamine (80 mg/kg) and xylazine (16 mg/kg) diluted in 0.9% saline. Eyedrops were used to dilate the pupils (1% tropicamide [NDC: 17478-102-12], 2.5% phenylephrine HCl [NDC: 17478-201-15], 1% cyclopentolate [NDC: 17478-096-15], all Akorn) and to anesthetize the corneal surface (0.5% proparacaine [HCl NDC: 17478-263-12], Akorn). Three electrodes were used to record ERGs. A thin stainless steel wire served as the active lead[34] and was coated at the end with 1% carboxymethylcellulose. Two Grass needle electrodes (Astro-Med, West Warwick, RI) served as the reference and ground leads and were placed in the cheek or tail, respectively. Strobe flash stimuli were presented in an LKC (Gaithersburg, MD) ganzfeld, first to the dark-adapted eye (−3.6 to 2.1 log cd s/$m^2$) and then superimposed upon a steady 20 cd/$m^2$ background field and after a 5-minute light adaptation period (−0.8 to 2.1 log cd s/$m^2$). ERGs were band-pass amplified (0.03 to 1000 Hz), averaged, and then stored using an LKC UTAS E-3000 signal averaging system.

The amplitude of the a-wave was measured at 8 ms after flash onset from the prestimulus baseline. The leading edge of the a-wave to a 1.4 log cd s/$m^2$ flash was measured using the equation:

$$P3(i,t) = \left(1 - \exp\left(iA(t - td)^2\right)\right) RmP3 \quad (1)$$

where *RmP*3 is the maximum response amplitude, *A* is a measure of sensitivity, and *td* is the delay in phototransduction.[35]

The amplitude of the b-wave was measured from the a-wave trough to the b-wave peak or, for low luminance flashes that do not elicit an a-wave, from the baseline to the peak of the b-wave. The function relating b-wave amplitude to flash luminance has two limbs.[36] We fit the first limb of this function using the Michaelis-Menten equation[37]:

$$R/R_{\max} = L/(L + K) \quad (2)$$

where $R$ is the amplitude of the a- or b-wave; $R_{\max}$ is the maximum amplitude of the a- or b-wave; $L$ is the flash energy (log cd s/m$^2$), and $K$ is the flash energy that elicits an amplitude of half $R_{\max}$ (half-saturation coefficient).

### 2.12 | Statistical analysis

Unpaired two-tailed Student's *t*-tests were done between two samples to determine the *P* values. One-way ANOVA was done when comparing more than two genotypes, and two-way ANOVA was done when comparing more than two different variables. Bonferroni's correction was done to determine the final *P* value. $P \leq .05$ was considered significant. All data in figures are mean ± SE N ≥ 3.

## 3 | RESULTS

### 3.1 | Generation and validation of the cell-specific Bsg knockout mouse

There are two splice variants of the *Bsg* gene, *Bsg1*, and *Bsg2* (Figure 1A). *Bsg1* includes exon 1A, which encodes for an additional Ig-domain that is not present in *Bsg2*. Previous studies have shown that *Bsg1* is preferentially expressed in photoreceptors, while *Bsg2* is widely expressed in most other cells.[38] *Bsg* floxed mice were generated by insertion of floxed sites on either side of exon 1.[26] Targeted deletion of exon 1 ensured that neither splice variant of *Bsg* would be expressed (Figure 1A).

BSG1 and BSG2 levels were examined in neural retina and RPE by preparing detergent soluble lysates from control or *NRL*$^{-/-}$ mouse eyes for western blot analysis (Figure 1B). In control neural retinas, the most prominent BSG1 band had a molecular weight of ~55 kD, similar to what was previously reported.[38] A second lighter band was observed above the prominent BSG1 band and was the only BSG1 band detected in lysates prepared from the *Nrl*$^{-/-}$ neural retina (Figure 1B left). The different mobilities of the BSG1 bands detected in rod-dominant control and cone-like photoreceptor dominant *NRL*$^{-/-}$ neural retinas suggest the two bands observed in the control retinas correspond to a rod-specific isoform (rBSG1) and a cone-specific isoform (cBSG1). The differences in band intensity for rBSG1 and cBSG1 in control retinas were consistent with the ratio of rods to cones, as rod photoreceptors make up a majority of the photoreceptor population.[39,40] To determine whether the difference in mobility of rBSG1 and cBSG1 resulted from differential glycosylation, lysates from control and *Nrl*$^{-/-}$ neural retinas were treated with PNGaseF to remove the N-linked oligosaccharides. After PNGaseF treatment, BSG1 from control and *Nrl*$^{-/-}$ neural retinas migrated with the same molecular weight, indicating that BSG1 is

differentially glycosylated in rod and cone photoreceptors (Figure 1B right). BSG1 was not detected in the RPE (Figure 1B). Differences were also found in the relative mobility of BSG2 between the neural retina and the RPE. After treatment with PNGaseF, the mobility of BSG2 was the same in the neural retina and the RPE (Figure 1B right).

To understand the importance of MCTs in supporting the metabolism of photoreceptors and the RPE, *Bsg* was selectively knocked out of rods (*RodΔBsg)*, cones (*ConeΔBsg)*, or RPE (*RPEΔBsg*) by crossing $Bsg^{flox/flox}$ mice with cell-specific *Cre* transgenic animals, as described in the Materials and Methods. We confirmed the cell-specific deletion of *Bsg* by western blot analysis of lysates prepared from control and cell-specific knockout mice (Figure 1C). The control neural retinal lysates yielded bands for rBSG1, cBSG1, and BSG2. Western blot analysis of *RodΔBsg* neural retinal lysates showed the rBSG1 band was absent, while the cBSG1 and BSG2 bands remained. In *ConeΔBsg* lysates, rBSG1 and BSG2 were present, while the cBSG1 band was diminished. Control RPE had a single BSG2 band, which was not detected in RPE lysates prepared from *RPEΔBsg* mice. These western blots confirmed the cell-specific deletion of BSG in the *RodΔBsg*, *ConeΔBsg*, and *RPEΔBsg* mouse lines.

### 3.2 | Characterization of the phenotype of RodΔBsg mouse

In the *RodΔBsg* neural retina, qPCR showed that *Bsg1* was decreased, while *Bsg2* and other members of the Ig superfamily were unchanged (Figure 2A), reflecting the expression of *Bsg2* in other cells in the neural retina including endothelial, Müller glia, astrocytes, and inner retinal neurons,[14,38] and the expression of *Bsg1* being restricted to photoreceptors as previously reported.[38] We used immunofluorescence confocal microscopy to examine the distribution of BSG and MCT1 in frozen retinal sections of eyes from control and *RodΔBsg* mice (Figure 2B). In the control retina, BSG and MCT1 co-localize in the inner segments, ONL, and the outer plexiform layer. When we examined the labeling pattern of BSG and MCT1 in *RodΔBsg* retinal sections, there was loss of BSG and MCT1 labeling of the plasma membrane of rod inner segments, while the heteromeric complex was still detected in the inner segments of cone photoreceptor cells (Figure 2B, asterisks). To confirm that the remaining BSG was from cone photoreceptors, *RodΔBsg* sections were co-labeled with BSG and cone arrestin (Supplemental Figure 1, asterisks). BSG labeling in the inner segments colocalized with cone arrestin, confirming BSG expression in cone photoreceptors of control and *RodΔBsg*. BSG staining in cones became more prominent in *RodΔBsg* compared to control, as rods account for a majority of the photoreceptors.[39,40] The remaining MCT1 and BSG labeling in the *RodΔBsg* ONL reflects the presence of these proteins in Müller cells and cones (Figure 2B). Some MCT1 staining was observed in inner segments lacking BSG (Figure 2B, arrows), suggesting that MCT1 synthesis continues in rods, but cannot be properly trafficked to the plasma membrane in the absence of BSG, as previously shown in vitro and in vivo.[10,11,13–15]

Western blot analysis of neural retina lysates from control and *RodΔBsg* mice showed a decrease in both MCT1 and MCT4 (Figure 2C,D). While our lab had previously demonstrated that MCT1 was expressed in photoreceptor cells, we were surprised to find MCT4 was also decreased in the retinal lysates prepared from *RodΔBsg* mice, as MCT4 was

reported to be restricted to Müller glial cells and inner retina.[41] This finding suggested that MCT4 was expressed in rod photoreceptors, so we queried publicly available RNA-seq data (GSE74660) for rod and *NRL*$^{-/-}$ photoreceptors.[42] The data showed high levels of *Slc16a1* expression (MCT1) in both rods and cones, while *Slc16a3* expression (MCT4) was higher in rods than in cones (Figure 2E).

To determine whether MCT4 protein was present in rod photoreceptor cells, we performed co-immunoprecipitation assays to determine if rBSG1 co-immunoprecipitated with MCT4. Detergent soluble retinal lysates were prepared from control and *RodΔBsg* mice and incubated with or without antibodies against MCT1 or MCT4. We found that rBSG1 co-immunoprecipitated with both MCT1 and MCT4 in control neural retina lysates, but not in *RodΔBsg* lysates (Figure 2F). These results confirm that rods express both MCT1 and MCT4 and that each transporter forms heteromeric complexes with rBSG1.

### 3.3 | Progressive photoreceptor degeneration in RodΔBsg retina

In vivo imaging was used to monitor longitudinal structural changes in retinas of *RodΔBsg* mice. BAF-cSLO images of *RodΔBsg* retinas show an age-related increase in hyperfluorescent foci (HF) in the subretinal space (Figure 3A). HF have been correlated with activation and migration of microglia and inflammatory monocytes into the subretinal space.[43–45] The appearance of HF in the *RodΔBsg* retina correlated temporally with altered photoreceptor OS morphology and significant thinning of the ONL and PL layers, observed via SD-OCT (Figure 3B,D,E) and histology (Figure 3C). These changes were not observed at 4 weeks of age (Figure 3D,E,F) but were already significant at 9 weeks of age and became more pronounced with age. By 35 weeks of age, the *RodΔBsg* ONL and PL layer was only ~60% of control. HF were not seen in 30-week-old control retinas but were pan-retinal in *RodΔBsg* retinas at that age. We also noted HF in mice at 35 weeks expressing only the *iCre* transgene, which may indicate a toxic effect of Cre recombinase for older rods. H&E stained histological sections also revealed disorganized OSs and the presence of cells within the OS layer of the older *RodΔBsg* mice (Figure 3C) that likely correspond to the HF seen by AF-SLO and are presumed to be inflammatory monocytes based on positive staining for Iba1 (data not shown ).

### 3.4 | Diminished ERGs in RodΔBsg mice

We used ERGs to evaluate overall retinal function in *RodΔBsg* mice. Figure 4A (left) presents representative ERGs obtained from *RodΔBsg* and control littermates at 17 weeks, an age where we see marked anatomical changes in the *RodΔBsg* retina (Figure 3). These responses were obtained under dark-adapted conditions and reflected primarily rod-mediated activity. The *RodΔBsg* responses contain the major ERG components, mainly reflecting the activity of rod photoreceptors (a-wave) or rod bipolar cells (b-wave). The amplitude of the overall *RodΔBsg* response is clearly reduced, with the magnitude of this reduction comparable across the stimulus range examined (Figure 4A right) and consistent with the loss of photoreceptors observed in vivo by SD-OCT and in histological sections (Figure 3).

To follow ERG changes with age in the *RodΔBsg* mice, we fit Equations (1) and (2) to the leading edge of the a-wave and the b-wave luminance-response function, respectively. At 4

weeks of age, the a-wave amplitude parameter *RmP3* was comparable in *RodΔBsg* and control mice (Figure 4B); *RmP3* values of *RodΔBsg* mice decreased steadily at later ages (Figure 4B) with a time course that mirrored the loss of rod photoreceptors (Figure 3D). The b-wave amplitude parameter $R_{max}$ was also reduced in *RodΔBsg* mice (Figure 4B), but the difference relative to control did not change with age to the extent seen for *RmP3*. At later ages the a-wave reductions were greater than the b-wave reductions, indicating that loss of MCT1 and MCT4 is more detrimental to light-stimulated OS responses than to the transmission of the visual signal from photoreceptors to bipolar cells, despite the loss of MCT1 and MCT4 in the outer plexiform layer of rod photoreceptors.

To examine the kinetics of the rod response, we superimposed the leading edge of normalized individual waveforms evoked by a high luminance flash (Figure 4C).[46] These waveforms were obtained from 4-week-old mice before the onset of ONL degeneration (Figure 3D). The kinetics of the *RodΔBsg* a-waves were slower than those of control responses, indicating that phototransduction gain was decreased in the absence of rBSG1 (Figure 4C) and a similar decrease was observed at all ages examined (Figure 4D). A similar analysis was not reported for the $Bsg^{-/-}$ mouse.[18,19]

In comparison to the changes noted for the dark-adapted ERG, cone ERG waveforms were similar between *RodΔBsg* and control mice at 17 weeks of age, and the cone ERG luminance response functions overlapped (Figure 4E). Cone ERGs of *RodΔBsg* mice decreased at later ages (Figure 4F), a change that is likely secondary to the progressive loss of rod photoreceptors (Figure 4D–F), which is seen in other models where the primary defect involves rods.[47]

### 3.5 | ERGs are not diminished in the MCT4$^{-/-}$ mouse

Since rod photoreceptors were found to express both MCT1 and MCT4, we could not distinguish which of these might play a more significant role in defining the phenotype observed in *RodΔBsg* mice. To address this, we characterized the retinal phenotype of $MCT4^{-/-}$ mice ($MCT1^{-/-}$ do not survive[48]). Western blot analysis showed that MCT4 was not detected in the $MCT4^{-/-}$ neural retina, while levels of rBSG1, cBSG1, and MCT1 were unchanged (Figure 5A). Since MCT4 is associated with a high rate of glycolysis and lactate production,[49,50] we examined lactate efflux in neural retinas isolated from control, $MCT4^{-/-}$, and *RodΔBsg* mice. There was no difference in lactate efflux between control and $MCT4^{-/-}$ mice (Figure 5B). In comparison, lactate efflux was reduced by 20% in the *RodΔBsg* retina (Figure 5B). We examined overall retinal function in the $MCT4^{-/-}$ mice at 6 months of age, where a clear phenotype was observed in *RodΔBsg* animals (Figures 3,4). ERGs of $MCT4^{-/-}$ mice were comparable to control under both dark-adapted (Figure 5C) and light-adapted (Figure 5D) conditions. These results indicate that the *RodΔBsg* phenotype does not reflect a dependence of rods on MCT4 and suggests that the phenotype is indicative of an essential role for MCT1 in rod photoreceptors.[51]

### 3.6 | Slow and incomplete loss of cone ERG amplitude in ConeΔBsg mice

Due to the low density of cone photoreceptors in the mouse retina, western blot and IHC did not easily detect changes in MCT1 levels in *ConeΔBsg* mice (Figure 1C). To visualize the

knockout of *Bsg* from cone photoreceptors by the *Opn1mw*cre transgene, *ConeΔBsg* mice and *RodΔBsg* mice were crossed to generate *Cone/RodΔBsg* mice. We co-stained BSG and cone arrestin, to confirm cone-specific knockout in *Cone/RodΔBsg* histological sections by the *Opn1mwcre* (Supplemental Figure 1). In comparison to control and *RodΔBsg* sections, there was no co-localization of BSG and cone arrestin in these sections, confirming cone-specific knockout of *Bsg* by the *Opn1mw-cre*. This finding, coupled with the western blot data (Figure 1C), demonstrates the *Opn1mw*-cre transgene effectively deleted *Bsg* expression from cone photoreceptors.

To confirm the deletion of *Bsg* from cone photoreceptors resulted in loss of MCT1 in cone photoreceptors, we compared the distribution of BSG and MCT1 labeling by immunofluorescence confocal microscopy on histological sections from *RodΔBsg* mice and *Cone/RodΔBsg*. BSG and MCT1 co-localized in cone inner segments of *RodΔBsg* mice (Figure 6A, asterisks), but were not detected in the inner segments of rods or cones in sections of eyes from the *Cone/RodΔBsg* mice (Figure 6B). The remaining staining of BSG and MCT1 in the ONL and inner segments of *Cone/RodΔBsg* mice must be from Müller cells, as *Bsg* was deleted from both rods and cones (Figure 6B, Supplemental Figure 1).

To examine the functional impact of deleting *Bsg* from cones, we used ERGs, which provide a sensitive measure of cone dysfunction,[52–54] to examine the *ConeΔBsg* mice. Under dark-adapted conditions, we noted no difference in the overall ERG waveform or amplitude (Figure 6C,D), indicative of spared rod pathway function at all ages examined. Under light-adapted conditions that isolate the cone pathway, ERGs of *ConeΔBsg* mice were only slightly reduced as compared to those obtained from control littermates at 17 weeks of age (Figure 6E). Across the age range examined, we noted that responses of *ConeΔBsg* mice were comparable to control at 4 and 9 weeks of age and were only slightly reduced at the later ages examined (Figure 6F). The reduction did not appear to become more pronounced with age, and **Rmax** values for the cone ERG luminance-response functions retained 84% of control values at 35 weeks of age (Figure 6F).

### 3.7 | Characterization of *RPEΔBsg* mice demonstrates an essential role for MCT1 and MCT3 maintaining the integrity and function of RPE and photoreceptor cells

The RPE expresses BSG2 (Figure 1B), which is required for maturation and trafficking of MCT1 and MCT3 to the apical and basolateral RPE membranes, respectively.[10,11,14] BSG2 is targeted to the basolateral membrane of the RPE through its association with MCT3 and to the apical membrane of the RPE through its association with MCT1, that lacks a basolateral sorting signal.[11] Since the *Best1-Cre* used here results in variable levels of *Cre* expression,[3,29] we restricted our analysis to *RPEΔBsg* mice with high levels of *Cre* expression (Figure 7A). Western blot analysis of RPE/choroid lysates from *RPEΔBsg* mice showed reduced levels of BSG2 as compared to control, as well as reduced levels of MCT1 and MCT3 (Figure 7B). At 17 weeks of age, SD-OCT images did not show thinning of the ONL or inner nuclear layer (INL) but showed areas of retinal detachment and OS disruption (Supplemental Figure 2). In older mice, at 43 weeks of age, BAF-cSLO showed increased HF in the *RPEΔBsg* retina (Figure 7C) while SD-OCT imaging revealed areas where the *RPEΔBsg* was detached (Figure 7D, red asterisk). *RPEΔBsg* mice had a thinned ONL,

disrupted and hypertrophic OSs, as well as inflammatory cells that were found in the subretinal space (Figure 7E). RPE flatmounts from *RPEΔBsg* revealed multiple abnormalities, including enlarged and irregularly shaped cells consistent with RPE stress[55] (Figure 7F).

ERGs were obtained from *RPEΔBsg* and control mice to determine the impact of *Bsg* deletion from the RPE on outer retinal function. *RPEΔBsg* mice had reduced ERGs under both dark-adapted (Figure 7G) and light-adapted (Figure 7H) conditions. These changes were noted in the youngest mice examined (4weeksold) and became more pronounced in older mice. Even at 17 weeks of age where there was no loss of ONL or INL, there was a severe reduction in ERG a- and b- wave amplitude, highlighting the importance of lactate transporters in the retina. Of all of the models examined in this project, the ERG changes noted in *RPEΔBsg* most closely matched those reported in the $Bsg^{-/-}$ model highlighted in Figure 8.[18, 19]

## 4 | DISCUSSION

Mice with a global genetic deletion of *Bsg* are infertile and have memory, immune, and visual deficits.[18] In the $Bsg^{-/-}$ mice, light- and dark-adapted ERGs are severely reduced as early as postnatal day 17, although photoreceptor cell degeneration is not apparent until after 8 weeks of age.[18,19] Previous studies from our lab linked the early visual deficits in the $Bsg^{-/-}$ mice to impaired trafficking of MCTs to the plasma membrane, resulting in impaired lactate transport within and out of the retina.[14] Findings from these studies demonstrated the overall importance of MCTs to maintaining the function and viability of photoreceptor cells but did not provide insight into which cells were driving the phenotype, as *Bsg* is expressed throughout the retina.

In our current study, we found the loss of photoreceptor function of the *RPEΔBsg* mouse most closely resembled the previously reported phenotype of the $Bsg^{-/-}$ mice. In Figure 8, ERG a-wave data from the $Bsg^{-/-}$ mice[19] was compared with the cell-specific *Bsg* knockout mice reported here. The reason that the deletion of *Bsg* from the RPE resulted in an early reduction of ERGs that mirrored the $Bsg^{-/-}$ phenotype[18,19] was most likely because of alterations to the microenvironment due to the inability of the RPE to regulate the lactate levels in the subretitinal space, impacting pH and osmolarity of the subretinal space (Figure 8 and Supplemental Figure 2). In contrast, the phenotypes of *RodΔBsg* and *ConeΔBsg* mice appeared much later and were less severe than was reported for $Bsg^{-/-}$ mice.[18,19] The *RodΔBsg* showed early reduction of ERG activity at 9 weeks of age, with the reduction in the a-wave correlating to rod photoreceptor death. These findings suggest that the dark-adapted ERG phenotype of the $Bsg^{-/-}$ was not due to energy deficits, but rather from alterations to the RPE. Additionally, *ConeΔBsg* did not show early loss of light-adapted (cone-driven) ERGs, suggesting that unlike rods, cone photoreceptors do not rely on lactate transport to maintain metabolic homeostasis and that ERG changes reported for $Bsg^{-/-}$ mice[18,19] were driven by changes in the RPE.

### 4.1 | The loss of Bsg in the RPE closely mimics the $Bsg^{-/-}$ phenotype

The RPE supports photoreceptor cell function including the visual cycle and the regulation of the transport of metabolites in and out of the subretinal space to meet the metabolic demands of the outer retina.[1,56] Glucose is the primary metabolic substrate of the outer retina where it is metabolized predominantly through aerobic glycolysis.[4] Excess lactate contributes to the metabolic coupling between the outer retina and the underlying RPE. The lactate generated by the retina is taken up by the RPE via MCT1, and then is either utilized for OXPHOS by the RPE to spare glucose for the outer retina[3,24,57] or it is transported across the basolateral membrane of the RPE by MCT3 to the choroidal capillaries.[10] The transepithelial transport of lactate out of the retina by the RPE maintains the lactate levels, pH, and osmolarity of the subretinal space.[10, 21, 22]

In *RPEΔBsg* mice, the loss of both MCT1 and MCT3 would be expected to prevent the transport of lactate, $H^+$, and $H_2O$ out of the subretinal space, thus altering the microenvironment of photoreceptors.[22] The retinas of *RPEΔBsg* exhibited a decrease in both rod and cone function as early as 4 weeks of age. At 17 weeks of age, the ONL and INL did not show changes in thickness, suggesting the ERG phenotype seen in *RPEΔBsg* and the $Bsg^{-/-}$ mice was driven by the changes in the microenvironment.[10,21,22] In vivo imaging by BAF-cSLO and histological sections showed invasion of immune cells into the subretinal space and disruption of OS structure. SD-OCT images from 17- and 43-week-old mice showed retinal detachment, consistent with fluid accumulation in the subretinal space as a consequence of the loss of MCTs, which coordinate the transport of fluid and lactate out of the subretinal space.[21]

In our previous study of the $Slc16a8^{-/-}$ ($MCT3^{-/-}$) mouse, the morphological and functional changes were not as severe as the *RPEΔBsg* mice,[10] which suggests that MCT1 expressed in the apical membrane of RPE, plays a significant role in regulating the lactate and $H^+$ levels in the subretinal space. MCT1 may plays an important role in maintaining the close association between the RPE and photoreceptor cells. SD-OCT imaging of the *RPEΔBsg* mice consistently showed detachment between the RPE and photoreceptors. This wasn't observed in histological sections of $Slc16a8^{-/-}$ mice, suggesting that MCT1 transport activity contributes to the movement of fluid out of the subretinal space.[21,22] This hypothesis is consistent with a recent analysis of GWAS data linking SNPs in *Slc16a1* (MCT1) with an increase in macular thickness. The same GWAS study, implicated MCT3 in macular thickening, as well as age-related macular degeneration (AMD)(GCST006976).[58] Our current studies and the finding from the GWAS study exemplify the importance of MCT1 and MCT3 for maintaining homeostasis in the outer retina.

The combined loss of MCT1 and MCT3 from the RPE may have a more severe phenotype than the $Slc16a8^{-/-}$ mice due to the multiple roles of MCT1 in the RPE. Lactate uptake from the subretinal space through MCT1 is utilized by the RPE to fuel OXPHOS, so glucose is spared for the outer retina. The RPE relies on OXPHOS to maintain its differentiation, as disruption of RPE mitochondria, or the TCA cycle enzyme has been linked to dedifferentiation of the RPE.[23,24] Loss of MCT1 in the *RPEΔBsg* mice could lead to nutritional deficits in the RPE, altering its oxidative capacity and shifting the balance between OXPHOS and glycolysis. This could lead to atrophy of the RPE and alterations to

RPE polarity, resulting in fluid accumulation in the subretinal space. In order to clarify the role of MCT1 in the RPE, future studies will characterize the retinal phenotype of MCT1 knock out of the RPE.

### 4.2 | The expression of MCT4 and glycolytic enzymes in rod photoreceptors

It has been reported in the literature that photoreceptor cells are dependent on aerobic glycolysis to support their anabolic and catabolic metabolism required for visual transduction and OS renewal.[59] Key enzymes involved in aerobic glycolysis, such as HK2, PKM2, and LDHA, have been found to be expressed in photoreceptors (Figure 2D,E).[59–64] In this study, we found rod photoreceptors express both MCT1 and MCT4, which are required for aerobic glycolysis.[49] Cone photoreceptors may also express both MCT1 and MCT4, but this will need to be further validated.

Previously, *Slc16a3* (encoding MCT4) expression had not been reported in neurons except under stressful conditions, for example, following ischemic stroke.[65] To our knowledge, this is the first time *Slc16a3* expression has been reported in neurons under homeostatic conditions. Characterization of $MCT4^{-/-}$ suggested that retinal MCT4 may not be needed under normal conditions, as ERG and lactate efflux did not change (Figure 5). *Slc16a3* (MCT4) has been shown to be under the transcriptional control of HIf1α in different tissues.[66,67] We speculate that due to the dense population of mitochondria in the inner segments, the mitochondria may generate metabolic intermediates or induce areas of low oxygen in the ONL that may stabilize HIf1α resulting in an upregulation of MCT4 expression, along with other glycolytic genes.[68,69]

In retinal disease models, MCT4 may play a larger role since photoreceptors under stress are more reliant on aerobic glycolysis for survival.[1,47,61,64] It has been suggested that upregulation of aerobic glycolysis in photoreceptors is required to preserve rod and cone photoreceptors under stressful conditions.[61,64] MCT4 may be required for lactate efflux under stress conditions, as MCT4 can export lactate in high-lactate environments.[50] It would be interesting to see the response of the retina in the $MCT4^{-/-}$ mouse under conditions of retinal stress, for example, after detachment or pharmacological insults, to understand the role of MCT4 in the retinal stress response.

### 4.3 | Lactate transporters are important to maintain rod photoreceptor activity and viability

Lactate is generated as the end-product of aerobic glycolysis, so we expected to find a decrease in lactate efflux in retinas from *RodΔBsg* mice. Lactate efflux measured in *ex vivo* assays from *RodΔBsg* retinas was only 20% less than the controls. Since rod photoreceptor cells constitute over 50% of the cell population in the neural retina,[39,40] we expected a higher decrease from *RodΔBsg* retinas. Similarly, the deletion of HK2 or PKM2 from rod photoreceptors resulted in a decrease in lactate efflux of less than 20% and 14%, respectively.[61,64] This suggests that rod photoreceptors may not be the primary lactate-producing cells in the neural retina, and that they both produce and utilize lactate, as previously reported.[20]

Despite the loss of lactate transport in *RodΔBsg* mice, the retinas developed normally as measured by OCT and ERGs at 4 weeks of age. However, the kinetics of the leading edge of the ERG a-wave were slowed (Figure 4C). Since rod photoreceptors are unable to either export or import lactate, this could be and early sign of metabolic dysregulation that is then followed by cell death (Figure 3D). Imported lactate could serve as a source of carbon for the TCA cycle that could be utilized to generate intermediates required for rod photoreceptor function.[20] Alternatively, the inability to export lactate could cause a buildup of lactate and $H^+$ in rods, leading to a decrease in the flux of glycolysis and an increase in the generation of reactive oxygenated species, causing cellular stress and eventual cell death. It is likely that a contribution of both scenarios are involved, as most cells rely on both OXPHOS and glycolysis, balancing the redox state and the energetic needs to maintain its metabolic homeostasis.[70]

It is interesting to note that while *RodΔBsg* showed an early functional phenotype at 4 weeks of age, *ConeΔBsg* exhibited only a mild phenotype at 17 weeks of age. This suggests that cone photoreceptors do not rely on lactate transport and aerobic glycolysis to maintain metabolic homeostasis. Based on findings from this study, and those from previous studies where metabolic enzymes were deleted in rods or cones or RPE,[3,61–63,71] it is tempting to speculate that rod photoreceptors are more sensitive to changes in aerobic glycolysis, while cone photoreceptors are reliant on OXPHOS and other substrates to maintain their metabolic needs.[72] This idea is consistent with our recent finding that glucose deprivation in the outer retina had a greater impact on rod than cone viability.[3] Future studies will investigate the possible metabolic differences between rod and cone photoreceptors and how the RPE meets the metabolic demands of both rods and cones.

## 5 | CONCLUSIONS

This study highlights the importance of MCTs in the RPE for maintaining lactate homeostatsis in the outer retina to support the function and viability of photoreceptors.

## Supplementary Material

Refer to Web version on PubMed Central for supplementary material.

## Funding information

HHS | NIH | National Eye Institute (NEI), Grant/Award Number: R01 EY12042; HHS | NIH | National Eye Institute (NEI), Grant/Award Number: P30 EY025585; U.S. Department of Veterans Affairs (VA), Grant/Award Number: I01 BX002340; HHS | NIH | National Institute on Alcohol Abuse and Alcoholism (NIAAA), Grant/Award Number: T32AA007463

## Abbreviations:

| | |
|---|---|
| **BSG** | basigin |
| **ERG** | electroretinogram |
| **INL** | inner nuclear layer |

| | |
|---|---|
| **MCT** | monocarboxylate transporter |
| **OCT** | optical coherence tomography |
| **ONL** | outer nuclear layer |
| **OS** | outer segment |
| **RPE** | retinal pigment epithelium |

## REFERENCES


1. Léveillard T, Philp NJ, Sennlaub F. Is retinal metabolic dysfunction at the center of the pathogenesis of age-related macular degeneration? Sci Int J Mol. 2019;20:762(1–20).
2. Joyal J-SS, Gantner ML, Smith LEH. Retinal energy demands control vascular supply of the retina in development and disease: the role of neuronal lipid and glucose metabolism. Prog Retin Eye Res. 2018;64:131–156. [PubMed: 29175509]
3. Swarup A, Samuels IS, Bell BA, et al. Modulating GLUT1 expression in retinal pigment epithelium decreases glucose levels in the retina: impact on photoreceptors and müller glial cells. Am J Physiol - Cell Physiol. 2019;316:C121–C133. [PubMed: 30462537]
4. Du J, Rountree A, Cleghorn WM, et al. Phototransduction influences metabolic flux and nucleotide metabolism in mouse retina. J Biol Chem. 2016;291:4698–4710. [PubMed: 26677218]
5. Basigin Muramatsu T. (CD147), a multifunctional transmembrane glycoprotein with various binding partners. J Biochem. 2016;159:481–490. [PubMed: 26684586]
6. Fisel P, Schaeffeler E, Schwab M. Clinical and functional relevance of the monocarboxylate transporter family in disease pathophysiology and drug therapy. Clin Transl Sci. 2018;11:352–364. [PubMed: 29660777]
7. Yoon H, Donoso LA, Philp NJ. Cloning of the human monocarboxylate transporter MCT3 gene: localization to chromosome 22q12.3-q13.2. Genomics. 1999;60:366–370. [PubMed: 10493836]
8. Philp NJ, Yoon H, Lombardi L. Mouse MCT3 gene is expressed preferentially in retinal pigment and choroid plexus epithelia. Am J Physiol Cell Physiol. 2001;280:C1319–C1326. [PubMed: 11287345]
9. Philp NJ, Wang D, Yoon H, Hjelmeland LM. Polarized expression of monocarboxylate transporters in human retinal pigment epithelium and ARPE-19 cells. Invest Ophthalmol Vis Sci. 2003;44:1716–1721. [PubMed: 12657613]
10. Daniele LL, Sauer B, Gallagher SM, Pugh EN, Philp NJ. Altered visual function in monocarboxylate transporter 3 (Slc16a8) knockout mice. Am J Physiol - Cell Physiol. 2008;295:451–457.
11. Castorino JJ, Deborde S, Deora A, et al. Basolateral sorting signals regulating tissue-specific polarity of heteromeric monocarboxylate transporters in epithelia. Traffic. 2011;12:483–498. [PubMed: 21199217]
12. Philp NJ, Yoon H, Grollman EF. Monocarboxylate transporter MCT1 is located in the apical membrane and MCT3 in the basal membrane of rat RPE. Am J Physiol-Regul Integr Comp Physiol. 1998;274:1824–1828.
13. Kirk P, Wilson MC, Heddle C, Brown MH, Barclay AN, Halestrap AP. CD147 is tightly associated with lactate transporters MCT1 and MCT4 and facilitates their cell surface expression. EMBO J. 2000;19:3896–3904. [PubMed: 10921872]
14. Philp NJ, Ochrietor JD, Rudoy C, Muramatsu T, Linser PJ. Loss of MCT1, MCT3, and MCT4 expression in the retinal pigment epithelium and neural retina of the 5A11/basigin-null mouse. Invest Ophthalmol Vis Sci. 2003;44:1305–1311. [PubMed: 12601063]
15. Gallagher SM, Castorino JJ, Wang D, Philp NJ. Monocarboxylate transporter 4 regulates maturation and trafficking of CD147 to the plasma membrane in the metastatic breast cancer cell line MDA-MB-231. Cancer Res. 2007;67:4182–4189. [PubMed: 17483329]

16. Rosell A, Meury M, AÍvarez-Marimon E, et al. Structural bases for the interaction and stabilization of the human amino acid transporter LAT2 with its ancillary protein 4F2hc. Proc Natl Acad Sci USA. 2014;111:2966–2971. [PubMed: 24516142]
17. Schmidt N, Kollewe A, Constantin CE, et al. Neuroplastin and basigin are essential auxiliary subunits of plasma membrane $Ca_2^+$ -ATPases and key regulators of $Ca^{2+}$ clearance. Neuron. 2017;96:827–838.e9. [PubMed: 29056295]
18. Hori K, Katayama N, Kachi S, et al. Retinal dysfunction in basigin deficiency. Investig Ophthalmol Vis Sci. 2000;41:3128–3133. [PubMed: 10967074]
19. Ochrietor JD, Moroz TP, Clamp MF, Timmers AM, Muramatsu T, Linser PJ. Inactivation of the Basigin gene impairs normal retinal development and maturation. Vision Res. 2002;42:447–453. [PubMed: 11853760]
20. Poitry-Yamate C, Poitry S, Tsacopoulos M. Lactate released by Muller glial cells is metabolized by photoreceptors from mammalian retina. J Neurosci. 1995;15:5179–5191. [PubMed: 7623144]
21. Adijanto J, Philp NJ. The SLC16A family of monocarboxylate transporters (MCTs)-physiology and function in cellular metabolism, pH homeostasis, and fluid transport. Curr Top Membr. 2012;70:275–312. [PubMed: 23177990]
22. Hamann S, Kiilgaard JF, La Cour M, Prause JU, Zeuthen T. Cotransport of $H^+$, lactate, and $H_2O$ in porcine retinal pigment epithelial cells. Exp Eye Res. 2003;76:493–504. [PubMed: 12634113]
23. Zhao C, Yasumura D, Li X, et al. mTOR-mediated dedifferentiation of the retinal pigment epithelium initiates photoreceptor degeneration in mice. J Clin Invest. 2011;121:369–383. [PubMed: 21135502]
24. Adijanto J, Philp NJ. Cultured primary human fetal retinal pigment epithelium (hfRPE) as a model for evaluating RPE metabolism. Exp Eye Res. 2014;126:77–84. [PubMed: 24485945]
25. Kurihara T, Westenskow PD, Gantner ML, et al. Hypoxia-induced metabolic stress in retinal pigment epithelial cells is sufficient to induce photoreceptor degeneration. Elife. 2016;5:1–22.
26. Bisetto S, Wright MC, Nowak RA, et al. New Insights into the lactate shuttle: role of MCT4 in the modulation of the exercise capacity. iScience. 2019;22:507–518. [PubMed: 31837519]
27. Li S, Chen D, Sauvé Y, McCandless J, Chen Y-J, Chen C-K. Rhodopsin-iCre transgenic mouse line for Cre-mediated rod-specific gene targeting. Genesis. 2005;41:73–80. [PubMed: 15682388]
28. Akimoto M, Filippova E, Gage PJ, Zhu X, Craft CM, Swaroop A. Transgenic mice expressing cre-recombinase specifically in M- or S-cone photoreceptors. Investig Ophthalmol Vis Sci. 2004;45:42–47. [PubMed: 14691152]
29. Iacovelli J, Zhao C, Wolkow N, et al. Generation of Cre transgenic mice with postnatal RPE-specific ocular expression. Investig Ophthalmol Vis Sci. 2011;52:1378–1383. [PubMed: 21212186]
30. Bisetto S, Whitaker-Menezes D, Wilski NA, et al. Monocarboxylate transporter 4 (MCT4) knockout mice have attenuated 4NQO induced carcinogenesis; A role for MCT4 in driving oral squamous cell cancer. Front Oncol. 2018;8:324. [PubMed: 30211114]
31. Wei H, Xun Z, Granado H, Wu A, Handa JT. An easy, rapid method to isolate RPE cell protein from the mouse eye. Exp Eye Res. 2016;145:450–455. [PubMed: 26424220]
32. Bell BA, Kaul C, Hollyfield JG. A protective eye shield for prevention of media opacities during small animal ocular imaging. Exp Eye Res. 2014;127:280–287. [PubMed: 25245081]
33. Bell BA, Bonilha VL, Hagstrom SA, Anand-Apte B, Hollyfield JG, Samuels IS. Prolonged ocular exposure leads to retinal lesions in mice. Exp Eye Res. 2019;185:107672(1–14). [PubMed: 31128100]
34. Goto Y An electrode to record the mouse cornea electroretinogram. Doc Ophthalmol J Clin Electrophysiol Vis-Off J Int Soc Clin Electrophysiol Vis. 1995;91:147–154.
35. Breton ME, Schueller AW, Lamb TD, Pugh EN. Analysis of ERG a-wave amplification and kinetics in terms of the G-protein cascade of phototransduction. Invest Ophthalmol Vis Sci. 1994;35:295–309. [PubMed: 8300357]
36. Peachey NS, Alexander KR, Fishman GA. The luminance-response function of the dark-adapted human electroretinogram. Vision Res. 1989;29:263–270. [PubMed: 2788958]
37. Fulton AB, Rushton WAH. Rod ERG of the mudpuppy: effect of dim red backgrounds. Vision Res. 1978;18:785–792. [PubMed: 676086]

38. Ochrietor JD, Moroz TP, Van Ekeris L, et al. Retina-specific expression of 5A11/Basigin-2, a member of the immunoglobulin gene superfamily. Investig Ophthalmol Vis Sci. 2003;44:4086–4096. [PubMed: 12939332]
39. Macosko EZ, Basu A, Satija R, et al. Highly parallel genome-wide expression profiling of individual cells using nanoliter droplets. Cell. 2015;161:1202–1214. [PubMed: 26000488]
40. Jeon CJ, Strettoi E, Masland RH. The major cell populations of the mouse retina. J Neurosci. 1998;18:8936–8946. [PubMed: 9786999]
41. Hoppe G, Yoon S, Gopalan B, et al. Comparative systems pharmacology of HIF stabilization in the prevention of retinopathy of prematurity. Proc Natl Acad Sci USA. 2016;113:E2516–E2525. [PubMed: 27091985]
42. Kim JW, Yang HJ, Oel AP, et al. Recruitment of rod photoreceptors from short-wavelength-sensitive cones during the evolution of nocturnal vision in mammals. Dev Cell. 2016;37:520–532. [PubMed: 27326930]
43. Bell BA, Kaul C, Bonilha VL, Rayborn ME, Shadrach K, Hollyfield JG. The BALB/c mouse: effect of standard vivarium lighting on retinal pathology during aging. Exp Eye Res. 2015;135:192–205. [PubMed: 25895728]
44. Flynn E, Ueda K, Auran E, Sullivan JM, Sparrow JR. Fundus autofluorescence and photoreceptor cell rosettes in mouse models. Investig Ophthalmol Vis Sci. 2014;55:5643–5652. [PubMed: 25015357]
45. Charbel Issa P, Barnard AR, Singh MS, et al. Fundus autofluorescence in the Abca4$^{-/-}$ mouse model of stargardt disease-correlation with accumulation of A2E, retinal function, and histology. Investig Ophthalmol Vis Sci. 2013;54:5602–5612. [PubMed: 23761084]
46. Hood DC, Birch DG. Assessing abnormal rod photoreceptor activity with the a-wave of the electroretinogram: Applications and methods. Doc Ophthalmol. 1996;92:253–267. [PubMed: 9476593]
47. Aït-Ali N, Fridlich R, Millet-Puel G, et al. Rod-derived cone viability factor promotes cone survival by stimulating aerobic glycolysis. Cell. 2015;161:817–832. [PubMed: 25957687]
48. Lee Y, Morrison BM, Li Y, et al. Oligodendroglia metabolically support axons and contribute to neurodegeneration. Nature. 2012;487:443–448. [PubMed: 22801498]
49. Tanner LB, Goglia AG, Wei MH, et al. Four key steps control glycolytic flux in mammalian cells. Cell Syst. 2018;7:49–62.e8. [PubMed: 29960885]
50. Contreras-Baeza Y, Sandoval PY, Alarcón R, et al. Monocarboxylate transporter 4 (MCT4) is a high affinity transporter capable of exporting lactate in high-lactate microenvironments. J Biol Chem. 2019;294:20135–20147. [PubMed: 31719150]
51. Peachey NS, Yu M, Han JYS, et al. Impact of MCT1 haploinsufficiency on the mouse retina In: Ash JD, Anderson RE,LaVail MM, Rickman CB, Hollyfield JG, Grimm C, eds. Advances in experimental medicine and biology, vol. 1074 New York LLC: Springer; 2018:375–380. [PubMed: 29721966]
52. Xu X, Quiambao AB, Roveri L, et al. Degeneration of cone photoreceptors induced by expression of the Mas1 protooncogene. Exp Neurol. 2000;163:207–219. [PubMed: 10785460]
53. Chang B, Hawes NL, Hurd RE, Davisson MT, Nusinowitz S, Heckenlively JR. Retinal degeneration mutants in the mouse. Vision Res. 2002;42:517–525. [PubMed: 11853768]
54. Chang B, Dacey MS, Hawes NL, et al. Cone photoreceptor function loss-3, a novel mouse model of achromatopsia due to a mutation in Gnat2. Investig Ophthalmol Vis Sci. 2006;47:5017–5021. [PubMed: 17065522]
55. Chen M, Rajapakse D, Fraczek M, Luo C, Forrester JV, Xu H. Retinal pigment epithelial cell multinucleation in the aging eye – a mechanism to repair damage and maintain homoeostasis. Aging Cell. 2016;15:436–445. [PubMed: 26875723]
56. Caceres PS, Rodriguez-Boulan E. Retinal pigment epithelium polarity in health and blinding diseases. Curr Opin Cell Biol. 2020;62:37–45. [PubMed: 31518914]
57. Kanow MA, Giarmarco MM, Jankowski CSR, et al. Biochemical adaptations of the retina and retinal pigment epithelium support a metabolic ecosystem in the vertebrate eye. Elife. 2017;6:1–25.

58. Gao XR, Huang H, Kim H. Genome-wide association analyses identify 139 loci associated with macular thickness in the UK Biobank cohort. Hum Mol Genet. 2019;28:1162–1172. [PubMed: 30535121]
59. Chinchore Y, Begaj T, Wu D, Drokhlyansky E, Cepko CL. Glycolytic reliance promotes anabolism in photoreceptors. Elife. 2017;6:1–22.
60. Lindsay KJ, Du J, Sloat SR, et al. Pyruvate kinase and aspartate-glutamate carrier distributions reveal key metabolic links between neurons and glia in retina. Proc Natl Acad Sci USA. 2014;111:15579–15584. [PubMed: 25313047]
61. Petit L, Ma S, Cipi J, et al. Aerobic glycolysis is essential for normal rod function and controls secondary cone death in retinitis pigmentosa. Cell Rep. 2018;23:2629–2642. [PubMed: 29847794]
62. Rajala A, Wang Y, Brush RS, et al. Pyruvate kinase M2 regulates photoreceptor structure, function, and viability. Cell Death Dis. 2018;9:240 (1–18). [PubMed: 29445082]
63. Rajala A, Wang Y, Soni K, Rajala RVS. Pyruvate kinase M2 isoform deletion in cone photoreceptors results in age-related cone degeneration. Cell Death Dis. 2018;9:737. [PubMed: 29970877]
64. Wubben TJ, Pawar M, Smith A, Toolan K, Hager H, Besirli CG. Photoreceptor metabolic reprogramming provides survival advantage in acute stress while causing chronic degeneration. Sci Rep. 2017;7:1–13. [PubMed: 28127051]
65. Rosafio K, Castillo X, Hirt L, Pellerin L. Cell-specific modulation of monocarboxylate transporter expression contributes to the metabolic reprograming taking place following cerebral ischemia. Neuroscience. 2016;317:108–120. [PubMed: 26751713]
66. Silagi ES, Novais EJ, Bisetto S, et al. Lactate efflux from intervertebral disc cells is required for maintenance of spine health. J Bone Miner Res. 2019:1–21.
67. Ullah MS, Davies AJ, Halestrap AP. The plasma membrane lactate transporter MCT4, but not MCT1, is up-regulated by hypoxia through a HIF-1α-dependent mechanism. J Biol Chem. 2006;281:9030–9037. [PubMed: 16452478]
68. Yu DY, Cringle SJ. Oxygen distribution in the mouse retina. Investig Ophthalmol Vis Sci. 2006;47:1109–1112. [PubMed: 16505048]
69. Iommarini L, Porcelli AM, Gasparre G, Kurelac I. Non-canonical mechanisms regulating hypoxia-inducible factor 1 alpha in cancer. Front Oncol. 2017;7:286 (1–8). [PubMed: 29230384]
70. Wilson DF. Programming and regulation of metabolic homeostasis. Am J Physiol Metab. 2015;308:E506–E517.
71. Kurihara T, Westenskow PD, Bravo S, Aguilar E, Friedlander M. Targeted deletion of Vegfa in adult mice induces vision loss. J Clin Invest. 2012;122:4213–4217. [PubMed: 23093773]
72. Perkins GA, Ellisman MH, Fox DA. Three-dimensional analysis of mouse rod and cone mitochondrial cristae architecture: bioenergetic and functional implications. Mol Vis. 2003;9:60–73. [PubMed: 12632036]

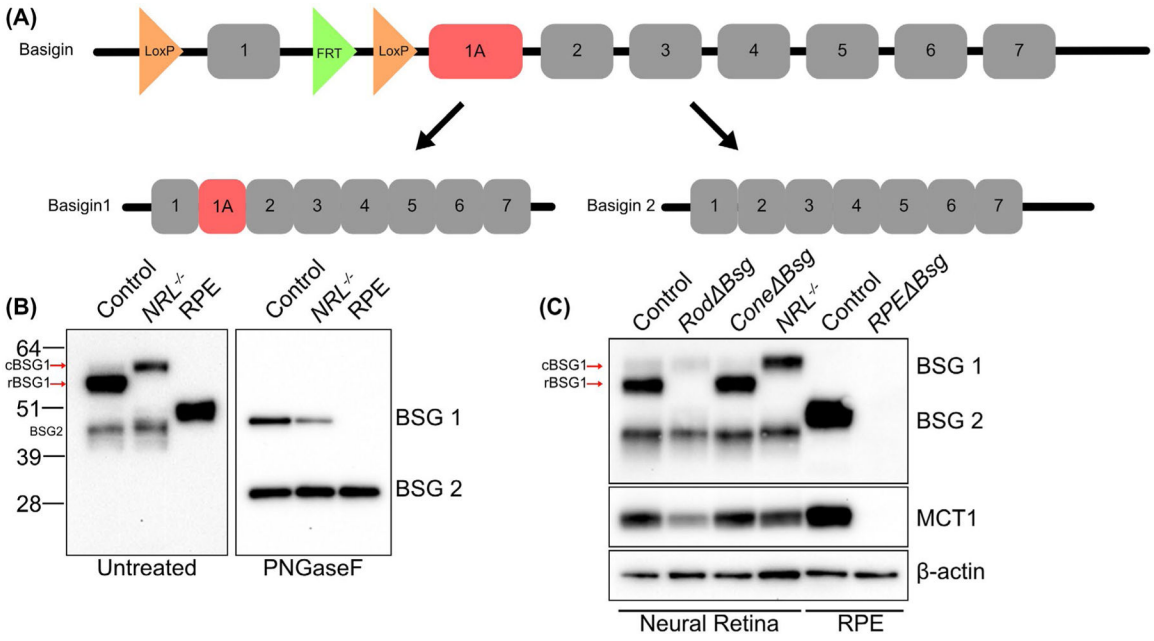


**FIGURE 1.**

Validation of mouse models with cell-specific deletion of Bsg in photoreceptors or RPE. A, Diagram of floxed *Bsg* gene and the splice variants *Bsg1* and *Bsg2*. LoxP sites were placed on either side of exon 1 so crossing the $Bsg^{flox/flox}$ mice with the cell-specific *Cre recombinase* transgenic lines resulted in loss of expression of both *Bsg1* and *Bsg2*. Exon 1A, present in *Bsg1* but not *Bsg2*, is highlighted in red. B, Western blot of detergent-soluble lysate from control retina, $NRL^{-/-}$ retina, and control RPE untreated (left) or after PNGaseF treatment (right). Note that rBSG1 is absent from the cone-rich $NRL^{-/-}$ retina and cone BSG1 (cBSG1) and rod BSG1 (rBSG1) from control retinas have different mobilities on SDS-PAGE in the untreated control samples but not after PNGaseF treatment. BSG2 between the neural retinas and the RPE also appear differentially glycosylated, but not after PNGaseF treatment. C, Western blot of detergent soluble retinal lysates from control, *RodΔBsg*, *ConeΔBsg*, and $NRL^{-/-}$ mice shows the rod-specific deletion of rBSG1 in *RodΔBsg* and cone-specific deletion of cBSG1 in *ConeΔBsg*. Western blot confirms the deletion of BSG2 from *RPEΔBsg* RPE. In B) and C) blots are representative of SDS-PAGE and blots performed on lysates from at least three animals per genotype

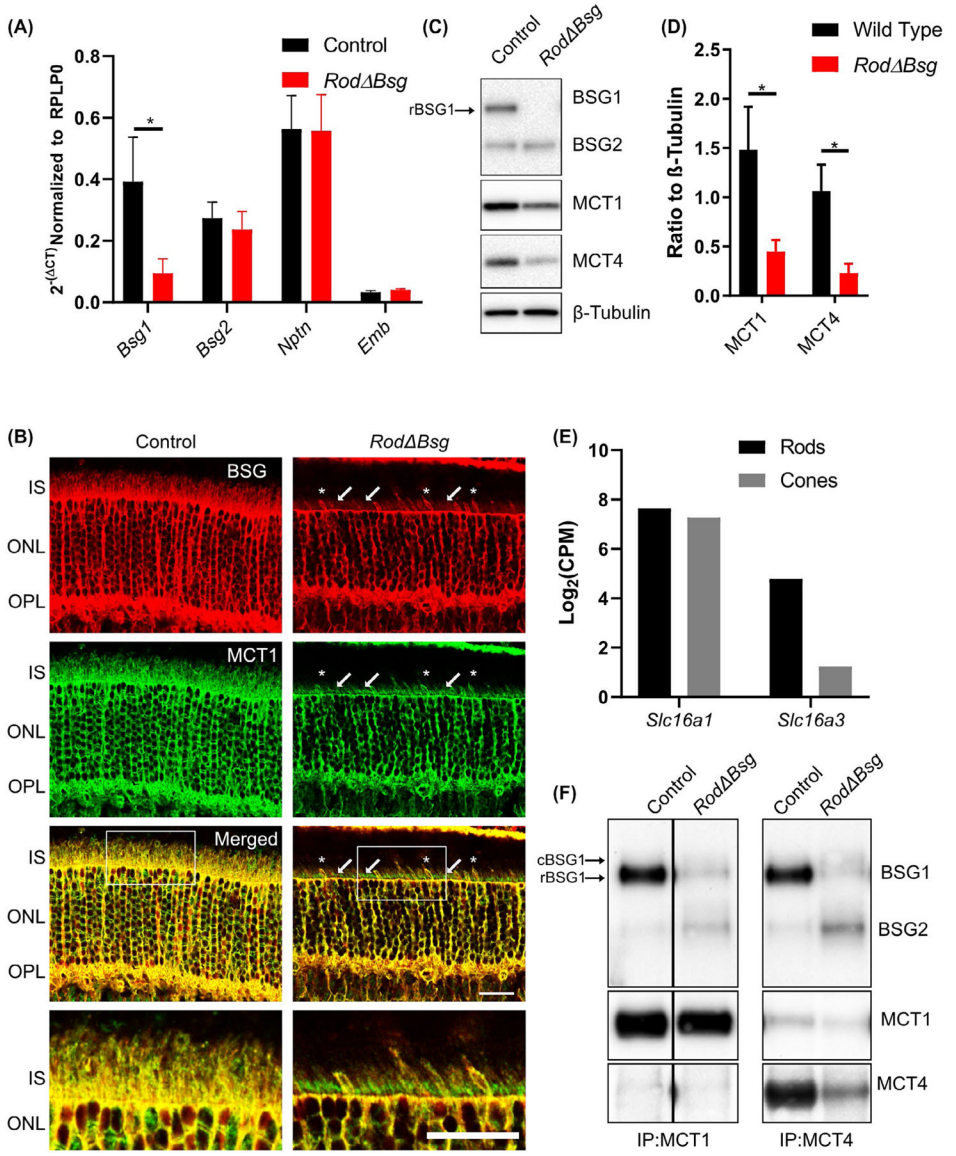


**FIGURE 2.**

rBSG1 is required MCT1 and MCT4 in rod photoreceptor cells. A, qPCR showing reduced levels of *Bsg1* in *RodΔBsg* retina without compensatory increases in levels of other Ig superfamily members. Bars indicate average ± SEM for N = 4 mice. B, Immunofluorescence of BSG (red) and MCT1 (green) of frozen sections of eyes from control and *RodΔBsg* mice. Loss of BSG1 resulted in loss of MCT1 in inner segments. MCT1 was still detected in rods (arrows) but was not trafficked to the plasma membrane (Scale bar = 25 μm). Asterisks indicate cones which retain both BSG1 and MCT1. Data are representative of N = 3 experiments. C, Western blots of detergent soluble lysates from *RodΔBsg* retinas confirms genetic deletion of *Bsg* from rod photoreceptors targets MCTs for degradation. Blots are representative of N = 8 mice. D, Western blot quantification of MCT1 and MCT4 compared to β-tubulin of control and *RodΔBsg* samples. E, Comparison of $Log_2$(CPM) values of *Slc16a1* (MCT1) and *Slc16a3* (MCT4) between rods and cones at P28 from GSE74660. F,

Immunoprecipitation of MCT1 and MCT4 shows enrichment of rBSG1 in control as compared to *Rod*Δ*Bsg* retina. Data are representative of N = 3 experiments

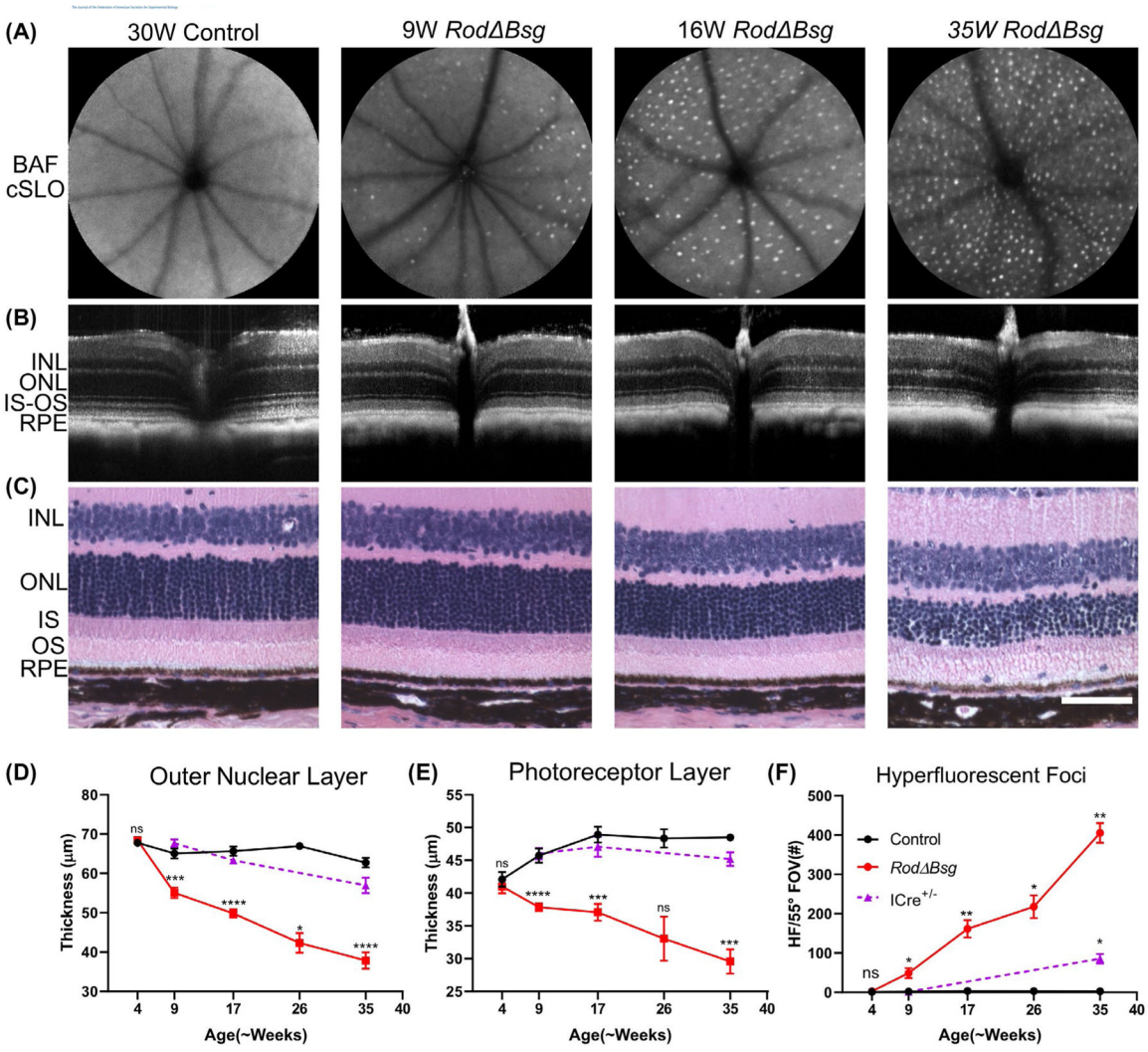


**FIGURE 3.**

Age-related structural changes in *RodΔBsg* retina. A, Blue-light autofluorescence cSLO imaging of control and *RodΔBsg* eyes and F) quantification of hyperfluorescent foci (HF), number of HF increased with age in *RodΔBsg* retina (average (±SEM) of N ≥ 3 mice per genotype). B, SD-OCT images of control and *RodΔBsg* eyes. C, Histology of paraffin section of eyes from control and *RodΔBsg* mice (scale bar indicates 50 μm). D, E, quantification of thickness of ONL and PL layers from SD-OCT images. Data points indicate average (±SEM) of N ≥ 3 mice

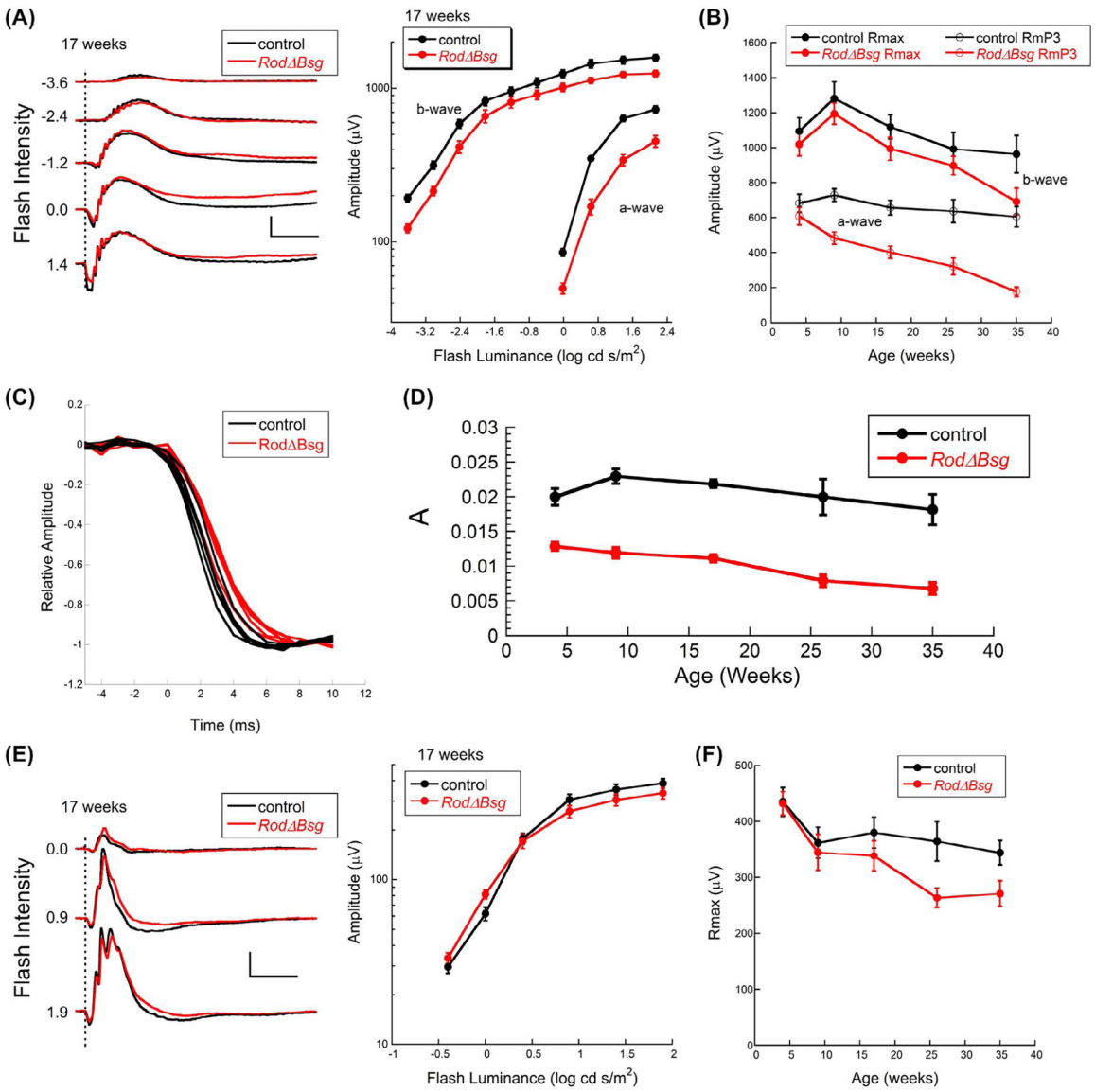


**FIGURE 4.**

Age-related changes in ERGs of *RodΔBsg* retina highlights importance of lactate transporters on rod photoreceptor function. A, Representative dark-adapted ERGs (left) and summary luminance-response functions from control and *RodΔBsg* littermates at 17 weeks of age. Values to the left of each pair of waveforms indicates flash strength in log cd s/m2. Calibration indicates 500 μV and 100 ms. B, Values of Rmax and RmP3 from control and *RodΔBsg* littermates at the ages indicated. C, Comparison of the leading edge of the a-wave of 4-week-old mice. For each mouse, amplitude was normalized to the a-wave trough. D, Values of A from control and *RodΔBsg* littermates at the ages indicated. E, Representative light-adapted ERGs (left) and summary luminance-response functions from control and *RodΔBsg* littermates at 17 weeks of age. Values to the left of each pair of waveforms indicates flash strength in log cd s/m$^2$. Calibration indicates 100 μV and 100 ms. F, Values of

Rmax for the cone ERG at the ages indicated. Data points indicate average (±SEM) for 4–7 mice

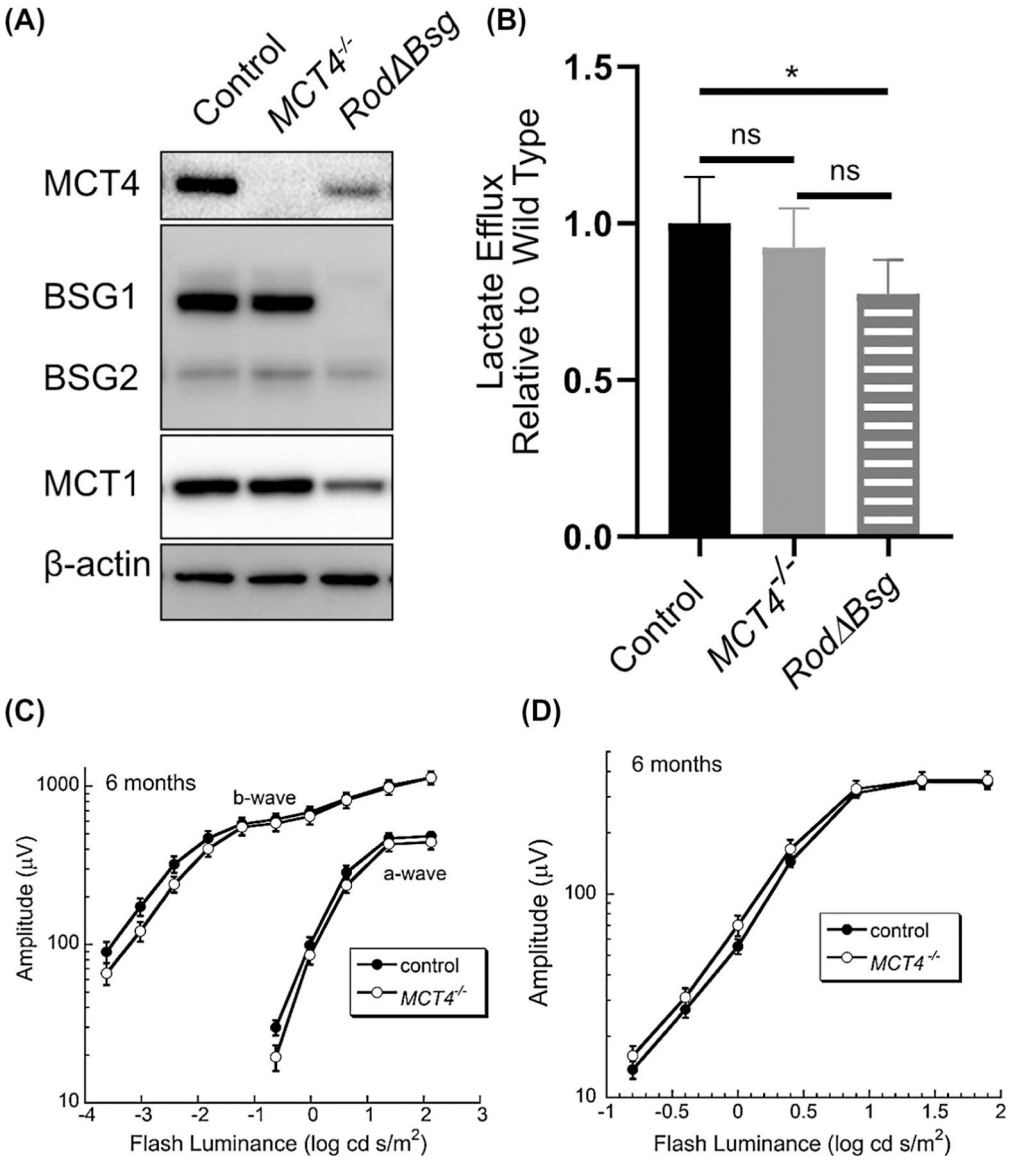


**FIGURE 5.**

Retinal phenotype of the *MCT4*$^{-/-}$ mouse A) Western blot analysis of control, *MCT4*$^{-/-}$, and *RodΔBsg* retinas. Blots are representative of N = 3 mice. B) Lactate efflux from control (N = 6), *MCT4*$^{-/-}$ (N = 3), and *RodΔBsg* retinas (N = 3). Luminance-response functions for the major components of the C) dark-adapted and D) light-adapted ERGs obtained from control and *MCT4*$^{-/-}$ mice. Data points indicate average (±SEM) for 12 mice

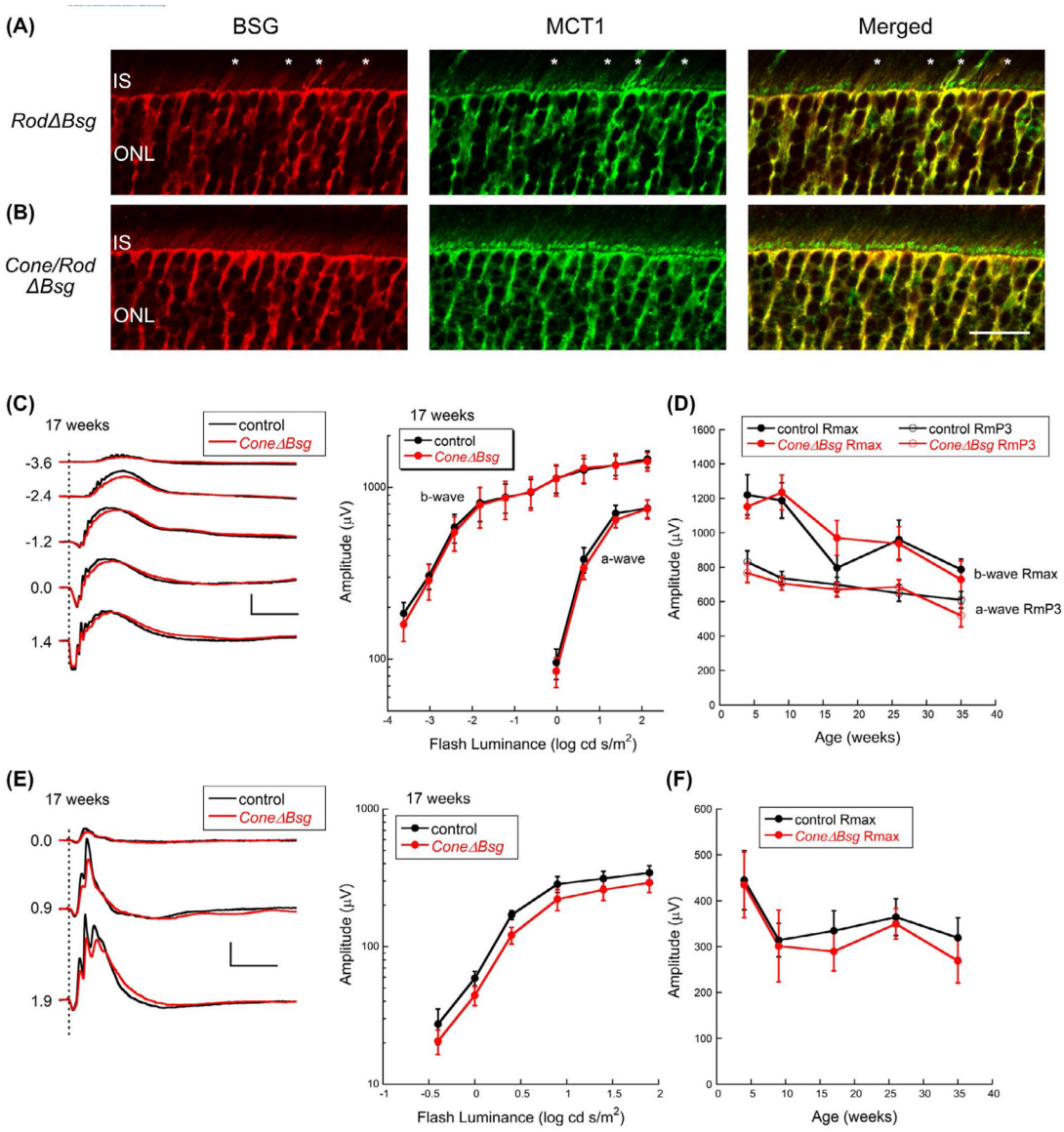


**FIGURE 6.**

Age-related changes in ERGs of *ConeΔBsg* retina. A, Immunofluorescence confocal microscopy of frozen sections of *RodΔBsg* and B, *Cone/RodΔBsg* eyes with BSG (red) and MCT1 (green) confirms BSG and MCT1 are not expressed in cone photoreceptors of *Opn1mwcre* transgenic mice (scale bar = 20 μm). C, Representative dark-adapted ERGs (left) and summary luminance-response functions (right) obtained from control and *ConeΔBsg* littermates at 17 weeks of age. Values to the left of each pair of waveforms indicates flash strength in log cd s/ $m^2$. Calibration indicates 500 μV and 100 ms. D, Values of Rmax and RmP3 from control and *ConeΔBsg* littermates at the ages indicated. E, Representative light-adapted ERGs from *ConeΔBsg* at 17 weeks of age. Values to the left of each pair of waveforms indicates flash strength in log cd s/$m^2$. Calibration indicates 100 μV and 100 ms. F, Values of Rmax for the cone ERG at the ages indicated. Data points indicate average (±SEM) for 6–9 mice

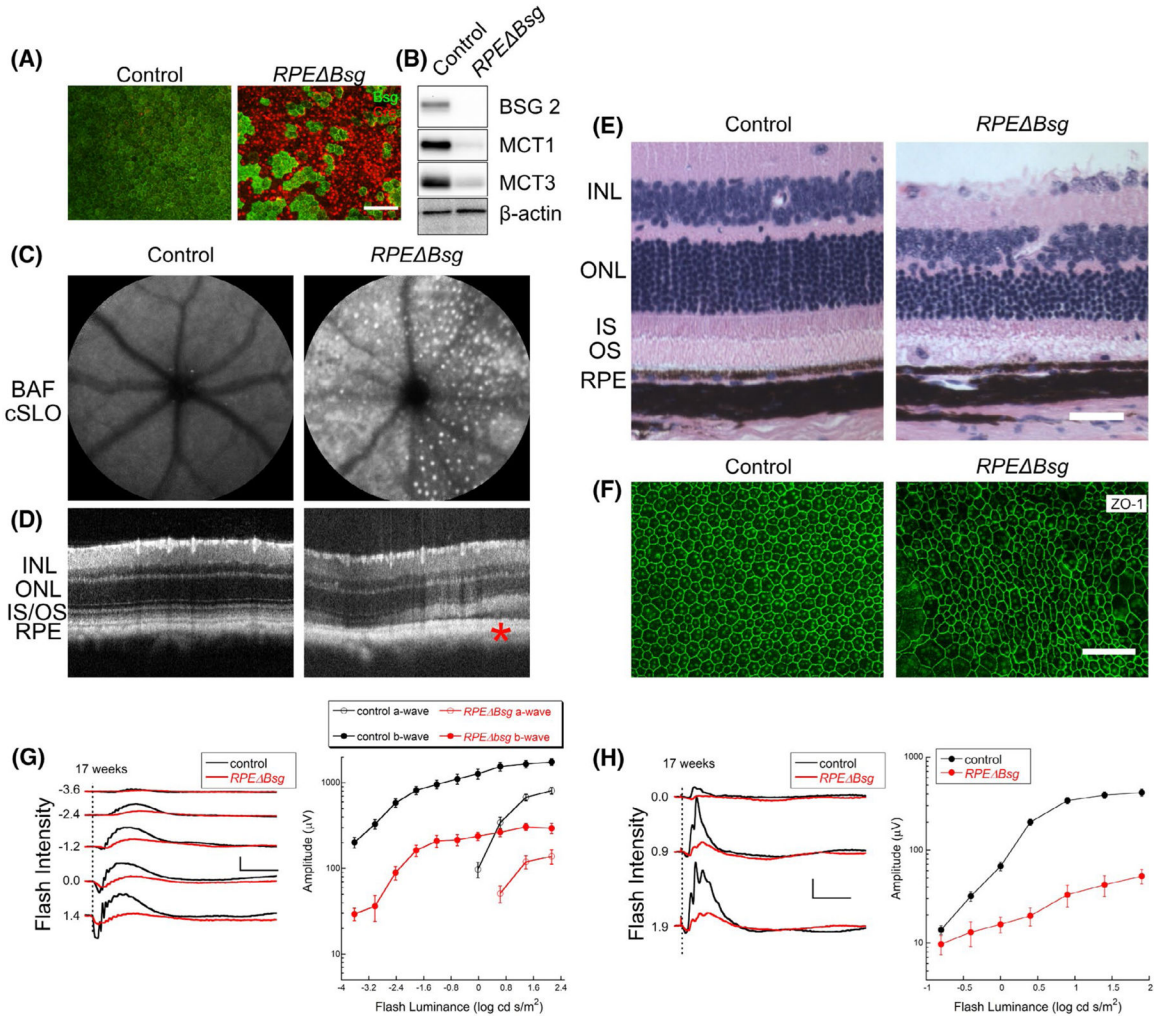


**FIGURE 7.**

RPE-specific deletion of BSG1. A, Immunofluorescent labeling of flatmounts of RPE from control and *RPEΔBsg* mice label with antibodies to BSG (green) and Cre (red) (scale bar = 100 μm). B, Western blot of lysates from control and *RPEΔBsg* RPE. C, BAF-cSLO demonstrates the increase in hyperfluorescent foci in *RPEΔBsg*. D, SD-OCT images of control and *RPEΔBsg* retina in 10-month-old *RPEΔBsg*. Red asterisk indicates retinal detachment. E, Representative H&E stained retinal cross sections of control and *RPEΔBsg* at 26 weeks of age (scale bar = 25 μm). F, Disorganized and enlarged RPE cells in *RPEΔBsg* flatmounts stained with ZO-1. All images are representative of N = 3 experiments (scale bar = 100 μm). Representative dark-adapted G) and light-adapted H) ERGs (left) and summary luminance-response functions right obtained from control and *RPEΔBsg* littermates at 17 weeks of age. Values to the left of each pair of waveforms indicates flash strength in log cd s/m$^2$. Calibration indicates 500 μV and 100 ms. Data points indicate average (±SEM) for 30 control and 6 *RPEΔBsg* mice

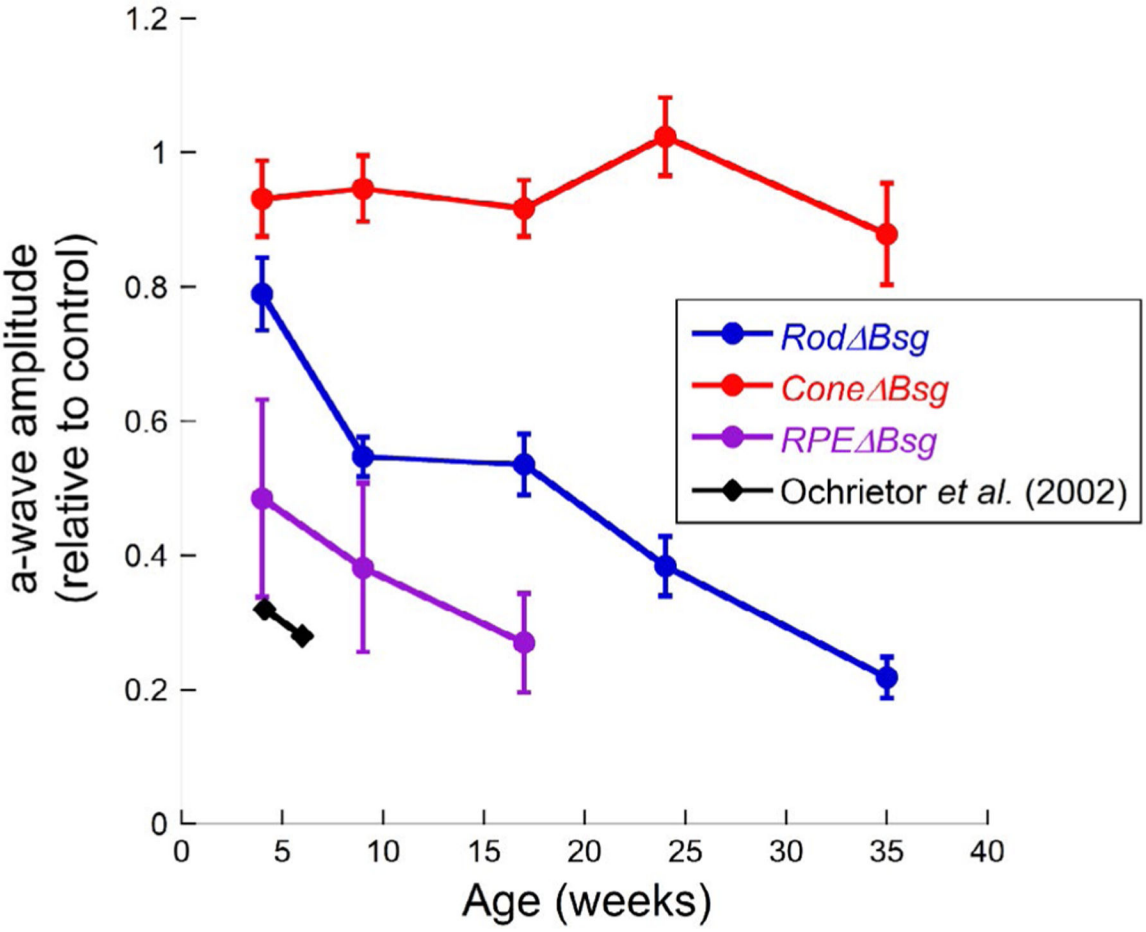


**FIGURE 8.**

Comparison of ERG a-wave changes in *Bsg*$^{-/-}$ cell-specific *Bsg* knockout mice. Summary of a-wave changes across the age range examined for *RodΔBsg* (Figure 4B), *ConeΔBsg* (Figure 6D), *RPEΔBsg* (Figure 7G), and *Bsg*$^{-/-}$[19]

**TABLE 1**

List of primers used for qPCR and genotyping

| Genes | Forward (5′–3′) | Reverse (5′–3′) |
|---|---|---|
| Bsg1 | GGA ATG CTC CAA ACG ACA GC | AGT AAG GTG GTT GCG GTC TG |
| Bsg2 | GGC GGG CAC CAT CCA AA | CCT TGC CAC CTC TCA TCC AG |
| Nptn | AAC CAG CTG GGC CAA TGA A | ACC AAA GAG GTC CAA GCA GAA |
| Emb | ATC GCT TAC GTG GGG GAT TC | GAG CGT CAA TGG GAA CCT GT |
| Rplp0 | AGATTCGGGATATGCTGTTGGC | TCGGGTCCTAGACCAGTGTTC |
| BSG Flox | GTA TAT GTG CTG CCG AAG CGA G | CAA AGC AGG TGG ACA GCC TAA TCT |
| Rho-iCre | TCA GTG CCT GGA GTT GCG CTG TGG | CTT AAA GGC CAG GGC CTG CTT GGC |
| Cre | ACTGGGATCTTCGAACTCTTTGGAC | GATGTTGGGGCACTGCTCATTCACC |
| Best-Cre | ATG CCC AAG AAG AAG AGG AAG GTG TCC | TGG CCC AAA TGT TGC TGG ATA GTT TTT A |
| MCT4 | GCA GCG CAT CGC CTT CTA TC | GTG TCA AGC TTA TGC CTG TC |

**TABLE 2**

List of antibodies used in this study and dilution

| Antibody | Company | Catalog | WB dilution | IF dilution |
|---|---|---|---|---|
| BSG(CD147) | Santa Cruz | Sc-9757 | 1:5000 | 1:500 |
| MCT1 | Philp Lab | (7–12) | 1:2000 | 1:250 |
| MCT3 | Philp Lab | (7–12) | 1:5000 | – |
| MCT4 | Philp Lab | (7–12) | 1:2000 | – |
| β-actin | Cell Signaling | 4967 | 1:2000 | |
| β-tubulin | Millipore Sigma | T4026 | 1:5000 | – |
| Cre | Millipore | MAB-3120 | – | 1:100 |
| Cone Arrestin | Millipore | AB15282 | – | 1:100 |
| ZO-1 | Zymed Laboratories Inc. | 61-7300 | – | 1:100 |
| Bovine anti-goat IgG-HRP | Jackson Immuno Research | 115-475-207 | 1:2000 | – |
| Goat anti-rabbit IgG-HRP | Jackson Immuno Research | 111-035-144 | 1:2000 | – |
| Alexa Fluor Donkey anti Rabbit 488 | ThermoFisher Scientific | A21206 | – | 1:500 |
| Alexa Fluor Donkey anti Goat 555 | ThermoFisher Scientific | A21432 | – | 1:500 |
| Alexa Fluor Donkey anti Mouse 546 | ThermoFisher Scientific | A10036 | – | 1:500 |